ARTICLE

doi:10.1038/nature14067

Endophilin marks and controls a clathrin-independent endocytic pathway

Emmanuel Boucrot[1,2], Antonio P. A. Ferreira[2], Leonardo Almeida-Souza[1], Sylvain Debard[2,3], Yvonne Vallis[1], Gillian Howard[1], Laetitia Bertot[4], Nathalie Sauvonnet[4] & Harvey T. McMahon[1]

Endocytosis is required for internalization of micronutrients and turnover of membrane components. Endophilin has been assigned as a component of clathrin-mediated endocytosis. Here we show in mammalian cells that endophilin marks and controls a fast-acting tubulovesicular endocytic pathway that is independent of AP2 and clathrin, activated upon ligand binding to cargo receptors, inhibited by inhibitors of dynamin, Rac, phosphatidylinositol-3-OH kinase, PAK1 and actin polymerization, and activated upon Cdc42 inhibition. This pathway is prominent at the leading edges of cells where phosphatidylinositol-3,4-bisphosphate—produced by the dephosphorylation of phosphatidylinositol-3,4,5-triphosphate by SHIP1 and SHIP2—recruits lamellipodin, which in turn engages endophilin. This pathway mediates the ligand-triggered uptake of several G-protein-coupled receptors such as α_{2a}- and β_1-adrenergic, dopaminergic D3 and D4 receptors and muscarinic acetylcholine receptor 4, the receptor tyrosine kinases EGFR, HGFR, VEGFR, PDGFR, NGFR and IGF1R, as well as interleukin-2 receptor. We call this new endocytic route fast endophilin-mediated endocytosis (FEME).

The BAR (Bin/amphiphysin/Rvs)-domain-containing protein endophilin-A (hereafter called endophilin) is an endocytic protein that recruits dynamin and synaptojanin[1], and the disruption of which has a profound effect on endocytosis in mice, nematodes and flies[2–5]. Evidence for its involvement in clathrin-mediated endocytosis came from BAR domain and antibody injection experiments in lamprey synapses, resulting in an accumulation of early- and late-stage clathrin-coated pits and a corresponding decrease in the number of synaptic vesicles[6–9]. Furthermore, endophilin has been detected on clathrin-coated pits by immuno-electron microscopy and fluorescence microscopy[5,9–12]. However, several lines of evidence suggest a peripheral role for endophilin in clathrin-mediated endocytosis: it was only detected in one-quarter of forming clathrin-coated pits[10,12]; triple knockdown (TKD) of all three endophilin-A proteins (A1, A2 and A3) by RNA interference (RNAi) does not affect the uptake of the clathrin-mediated endocytosis cargo transferrin[13]; and the kinetics of synaptic vesicle retrieval in goldfish bipolar neurons inhibited by endophilin N-BAR domain injection (BAR domain with its amino-terminal amphipathic helix extensions) was distinct from that inhibited by a peptide inhibitor of clathrin-mediated endocytosis[14,15]. Interestingly, endophilin binds directly to a proline-rich motif present in the third intracellular loop (TIL) of the β_1-adrenergic receptor (β_1-AR) but not the β_2-AR (ref. 16), both being members of the G-protein-coupled receptor (GPCR) superfamily. Endophilin also binds to EGFR and HGFR through CIN85 and Cbl (refs 17, 18). Here we reveal that endophilin is not simply a peripheral component of clathrin-mediated endocytosis but principally marks and controls a distinct endocytic pathway.

Endophilin-dependent endocytosis of GPCR

Looking for cargoes that can bind to the SH3 domain of endophilin, we found that in addition to β_1-AR, endophilin bound strongly to discrete proline-rich motifs within the TIL of the α_{2a}-AR, dopaminergic receptors 3 and 4 (DR3 and DR4) and to the muscarinic acetylcholine receptor 4 (mAchR4), and weakly to the histaminergic receptors 1 and 3 but not to the other members of the amine GPCR sub-family tested (Fig. 1a and Extended Data Fig. 1a–e). The internalization of β_1-AR in an antibody-feeding assay was strongly decreased in endophilin TKD but not in clathrin or AP2-depleted cells, suggesting an endocytic route independent of clathrin-mediated-endocytosis (Fig. 1b). Among the five endophilin genes, A2 was the most important in BSC1 cells, followed by A1, with little or no role for A3, B1 and B2. The uptake of β_1-AR required full-length A2 and its N-BAR or SH3 domains could not rescue the endophilin TKD (Fig. 1b). Consistent with the binding data, only internalization of β_1-AR and α_{2a}-AR, DR3, DR4, and mAchR4 was significantly reduced in endophilin TKD cells (Extended Data Fig. 1m, n). These endocytic defects were only observed after ligand stimulation, implicating endophilin in receptor-mediated endocytosis initiated upon receptor activation by their ligands. Endophilin TKD cells showed unperturbed uptake of transferrin and LDL receptors (cargo for clathrin-mediated endocytosis), but clathrin-coated pits formed at a slightly slower rate (Extended Data Fig. 1f–i), perhaps related to a reduced synaptojanin recruitment to membranes and thus an increase in phosphatidylinositol-4,5-bisphosphate (PtdIns(4,5)P_2) levels[5,19]. Surface β_1-AR accumulated mostly at the leading edge of endophilin TKD cells, which coincided with the localization of most of the endophilin signal in control cells (Fig. 1c, Extended Data Figs 1j–l and 2 and Supplementary Video 1). Consistent with the virtual absence of clathrin-coated pits and vesicles at the leading edge (Extended Data Fig. 2e), endogenous endophilin showed little co-localization with AP2 ($2 \pm 0.1\%$ of endogenous AP2 spots), much lower than observed for endophilin overexpression data ($\sim$5% on snapshot confocal images and a brief flash just before budding in $\sim$25% of recorded clathrin-coated vesicle budding kymographs, in agreement with previous studies[10,12]). In confluent cells, which lack leading edges, endophilin puncta were interspersed with clathrin-coated pits on the ventral surface (Extended Data Fig. 2i, j and Supplementary Video 2).

Endophilin co-localized at the leading edge with its binding proteins (dynamin, synaptojanin, lamellipodin) and with F-actin but not with the clathrin-independent endocytic proteins caveolin-1, flotillin1/2 or

[1]MRC Laboratory of Molecular Biology, Francis Crick Avenue, Cambridge CB2 0QH, UK. [2]Institute of Structural and Molecular Biology, University College London & Birkbeck College, London WC1E 6BT, UK. [3]Department of Biology, Ecole Normale Supérieure de Cachan, 94235 Cachan, France. [4]Institut Pasteur, Unité de Pathogenie Moleculaire Microbienne, 28 rue du Docteur Roux, 75724 Paris Cedex 15, France.

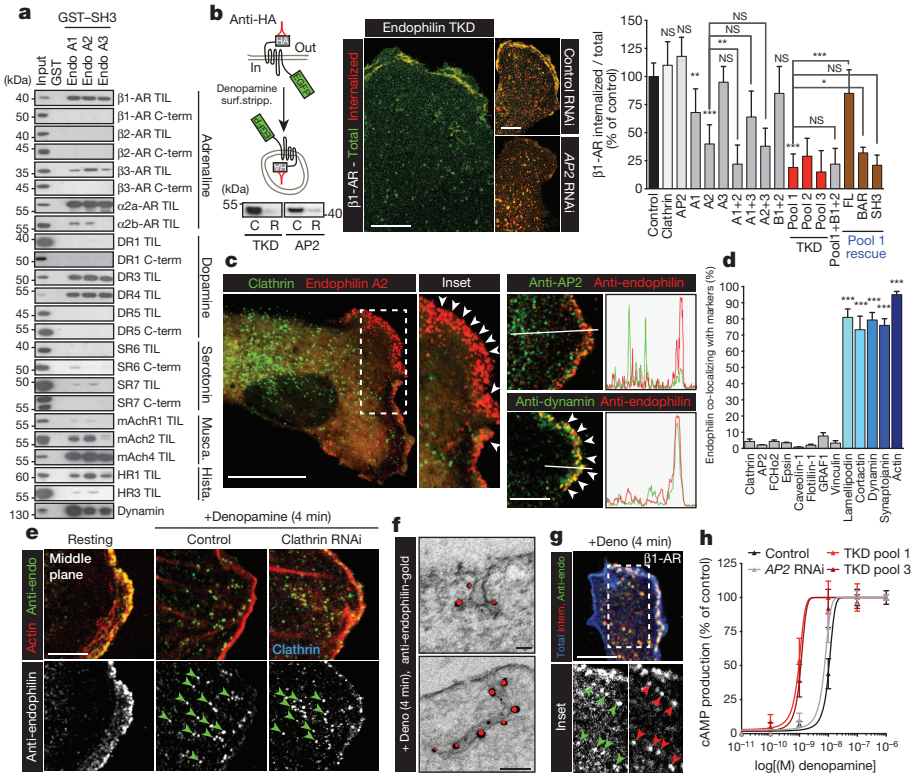

Figure 1 | Clathrin-independent, endophilin-dependent endocytosis of GPCR. **a**, Pull-down experiments with EGFP-tagged third intracellular loops (TIL) or C termini of indicated GPCRs. **b**, Left: antibody feeding assay using double-tagged β_1-AR. HA antibodies are internalized after denopamine stimulation and non-internalized antibody was removed by surface stripping (surf.stripp.). Bottom: immunoblots from control (C) and RNAi (R) endophilin TKD and AP2-depleted cells. Right: confocal microscopy images of internalized (red) and total (green) HA–β_1-AR–EGFP (images are representative of at least ten captures from three independent experiments). Bar graphs show the amounts of internalized receptors corrected for their total levels in the indicated samples (means ± s.e.m. from three independent experiments; NS, non-significant; $*P < 0.05$, $**P < 0.01$, $***P < 0.001$; one-way ANOVA and Dunnett's test versus control or versus A2 or TKD pool 1, as indicated by the brackets). FL, full length. **c**, Confocal sections showing localization of endophilin-A2–RFP (left) or endogenous endophilin (right) with clathrin (EGFP–LCa), AP2 or dynamin in BSC1 cells (images are representative of at least ten captures from three independent experiments). Intensity profiles were acquired along the indicated lines. Arrowheads show leading edge. **d**, Percentage of endogenous endophilin spots co-localizing with the named markers (means ± s.e.m. from three independent experiments; $***P < 0.001$, one-way ANOVA and Dunnett's test versus control IgG). **e**, Confocal sections of cells immunostained for endophilin (green) and actin (red) following the indicated treatments. Arrowheads show endophilin-positive assemblies (EPAs) (images are representative of at least ten captures from three independent experiments). **f**, Immuno-electron microscopy of BSC1 cells immunostained for endophilin (red) (images are representative of ten captures from two independent experiments). **g**, Co-staining of internalized β_1-AR and endogenous endophilin after stimulation. Blue, total β_1-AR (images are representative of ten captures from two independent experiments). **h**, cAMP production following stimulation with denopamine (means ± s.e.m. from three independent experiments). Scale bars: 20 μm (**c**, left), 10 μm (**b**), 5 μm (**c**, right, **e**, **g**) and 250 nm (**f**).

GRAF1 (refs 20–22) (Fig. 1c, d and Extended Data Fig. 3). As the depletion of the latter did not affect endophilin signals or internalization of the five GPCRs identified, it suggested a hitherto novel endocytic process.

Very shortly ($t_{1/2} = 7$ s) after addition of β_1-AR but not β_2-AR agonists, numerous endophilin–RFP-positive assemblies (EPAs) emanated from the cell edges and rapidly (1.62 ± 0.29 μm s^{-1}) travelled to the perinuclear area (Extended Data Fig. 4a, b and Supplementary Video 3). The formation of intracellular tubules and vesicles positive for endogenous endophilin after β_1-AR-specific activation was confirmed by confocal and electron microscopy (Fig. 1e–g and Extended Data Fig. 4c–o). EPAs were quantified on middle confocal planes and the vesicles/tubules formed were probably detached as they were no longer accessible to externally applied dyes.

Consistently with the absence of co-localization, EPA formation was unaffected by the inhibition of clathrin-mediated endocytosis by AP180 carboxy terminus overexpression or by RNAi of the clathrin-mediated endocytosis components clathrin heavy chain or AP2 (Extended Data Fig. 4g and j). As expected from the binding data, only the overexpression of TILs from the receptors that bound to endophilin perturbed EPA formation (Extended Data Fig. 5a, b). EPAs formed upon β_1-AR activation were confirmed as authentic endocytic carriers because in the antibody-feeding assay they contained anti-HA antibodies (Fig. 1g).

Finally, signal transduction downstream of β_1-AR (cAMP production and PKA-mediated CREB phosphorylation) was elevated in endophilin TKD cells (Fig. 1h and Extended Data Fig. 5c, d), suggesting that EPAs mediate the downregulation of activated β_1-AR. Even though β-arrestin, a key clathrin-mediated endocytosis adaptor for β_2-AR, was located at the edge of cells, it was not detected on EPAs, nor did its overexpression or depletion perturb EPA formation after β_1-AR stimulation (Extended Data Fig. 5e–h). Given that these EPAs form rapidly in an actin- and dynamin-dependent manner (see below), we named this new, clathrin-independent internalization route fast endophilin-mediated endocytosis (FEME), as distinct from clathrin-mediated endocytosis (CME).

Receptor-tyrosine kinase uptake by FEME

As removal of serum (hence of growth factors) from the culture medium or addition of extra serum strongly decreased or increased, respectively, the formation of EPAs (Fig. 2a), we assessed the capacity of various growth factors to activate FEME. Addition of EGF, HGF, FGF, VEGF, PDGF, NGF and IGF-1 but not TGF-β or BMP2 induced the formation of EPAs in three different cell lines, including primary fibroblasts from adult donors (Fig. 2a–c, Extended Data Fig. 6a–d and Supplementary Video 4). EGF induced the formation of EPAs in a dose-dependent manner and for prolonged periods of time. Fluorescently

labelled EGF or antibodies specific to the extracellular part of EGFR added to the extracellular medium, but not the β_1-AR, could be detected within EPAs only upon stimulation with EGF (Fig. 2d, e and Extended Data Fig. 6e), establishing that a receptor must be activated by its cognate ligand to become a FEME cargo.

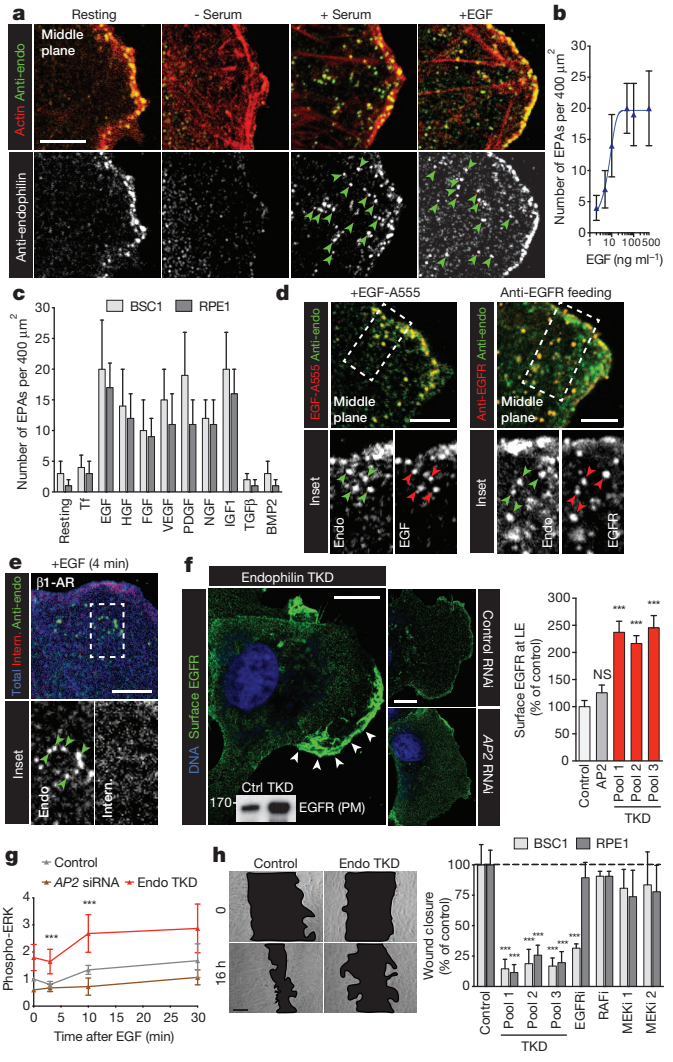

Figure 2 | Endocytosis of RTKs by the FEME pathway. **a**, Confocal sections of cells immunostained for endophilin and actin following the indicated treatments. Arrowheads show EPAs. Images are representative of at least ten captures from three independent experiments. **b**, **c**, Quantification of the number of EPAs after 4 min stimulation with various EGF concentrations (**c**) or 10 ng ml^{-1} of the indicated growth factors (means ± s.e.m. from three independent experiments). **d**, **e**, Co-staining of internalized Alexa555-labelled EGF (**d**, left), anti-EGFR antibody (+EGF; **d**, right) or β_1-AR (+EGF; **e**) and endogenous endophilin. Arrowheads show EPAs (images are representative of ten captures from three independent experiments). **f**, Cell surface staining of endogenous EGFR in resting control, AP2 or endophilin TKD cells (images are representative of ten captures from three independent experiments). Immunoblot shows the amount of EGFR in plasma membrane (PM) fractions of control or endophilin TKD cells. Bar graph shows the quantification of surface EGFR signals at the cell leading edge (LE) in the indicated conditions (means ± s.e.m. from three independent experiments; NS, non-significant; ***$P < 0.001$, one-way ANOVA and Dunnett's test versus control). **g**, Levels of phosphorylated Erk1/2 in control, *AP2* RNAi or TKD cells upon stimulation with 5 ng ml^{-1} EGF, determined on immunoblots (means ± s.e.m. from three independent experiments; ***$P < 0.001$, one-way ANOVA and Dunnett's test versus control $t = 0$). **h**, Cell migration into wound sites in samples treated with the indicated RNAi or inhibitors (means ± s.e.m. from three independent experiments; ***$P < 0.001$, one-way ANOVA and Dunnett's test versus respective control). Scale bars: 20 µm (**h**), 10 µm (**f**) and 5 µm (**a**, **d**, **e**).

Consistent with the binding of endophilin to EGFR and HGFR through CIN85 and Cbl (refs 17,18), depletion of CIN85 or Cbl, or overexpression of a mutant form of CIN85 (which binds Cbl but not endophilin), inhibited EPA formation upon EGF or HGF stimulation but not β_1-AR stimulation (Extended Data Fig. 6f).

EGFR, similarly to β_1-AR, accumulated at the plasma membrane of endophilin TKD cells (Fig. 2f), which resulted in elevated downstream MAPK signalling during the first 10 min of stimulation (Fig. 2g and Extended Data Fig. 7a–g), indicating that endophilin was necessary for maintaining a low basal activation state.

We found that concentrations of EGF over 5 ng ml^{-1} were required for full stimulation of EPAs (Fig. 2b), consistent with dynamin-dependent, clathrin-independent endocytic pathway(s) downregulating EGFR signalling at these concentrations[23] (clathrin-mediated endocytosis can function at ≤2 ng ml^{-1} EGF concentrations). However, MAPK signalling was downregulated in endophilin TKD cells upon 30 min of high (100 ng ml^{-1}) EGF stimulation (Extended Data Figs 6g–j and 7c), indicating that another endocytic process, probably macropinocytosis, is then mediating EGFR uptake. Notably, FEME carriers and macropinocytosis co-exist but are morphologically distinct—small, <1 µm, tubules and vesicles compared with large (2–10 µm) ruffles and pinosomes (Extended Data Fig. 6k).

The very prompt budding of endocytic vesicles following receptor stimulation and the enrichment of endophilin at the leading edge suggests that FEME might be involved in directed cell migration. Similarly to EPA formation, migration of endophilin TKD cells was strongly decreased in an EGFR-dependent, but RAF- and MEK-independent, manner (Fig. 2h and Extended Data Fig. 7h), suggesting separate functions for FEME in MAPK signalling and cell migration downstream of EGFR. Finally, consistent with the decrease in NGFR uptake, neurite extension in response to NGF was strongly inhibited in endophilin TKD PC12 cells (Extended Data Fig. 7i–k), consolidating a role for FEME in growth-factor signalling and cell migration.

IL-2 receptor endocytosis by FEME

We next investigated which known clathrin-independent cargoes could use the FEME pathway to enter cells. The β-chain of the interleukin-2 receptor (IL-2Rβ) and the common cytokine γ-chain (IL-2Rγc) are known to use a clathrin-independent endocytic route[24,25]. The IL-2 receptor (composed of the IL-2Rα, β and γc chains) assembles upon binding to IL-2, triggering a signal transduction cascade leading to lymphocyte proliferation and immune responses. After addition of 200 pM IL-2 together with an antibody specific to the extracellular domain of IL-2R, numerous EPAs containing internalized antibodies were observed in a human T-cell line (Fig. 3a, b). Upon addition of IL-2, endophilin puncta were observed at the edges of cells, followed by numerous internal EPAs (Extended Data Fig. 8a, b). However, we did not detect significant co-localization of endophilin with 16 transmembrane and glycophosphatidylinositol (GPI)-anchored receptors of the cluster of designation (CD) superfamily known to be internalized by clathrin-independent mechanisms[26] (Fig. 3a). Consistently, endophilin TKD only decreased the endocytic rate of IL-2R but not that of the other receptors (Fig. 3c). Together, this demonstrated that the FEME pathway mediates the uptake of IL-2-triggered IL-2R but that not all clathrin-independent cargo use this internalization pathway.

Inhibitors of the FEME pathway

Inhibition of clathrin-mediated endocytosis using five different genetic approaches (RNAi of key components or overexpression of dominant-negative mutants) did not interfere with EPA production upon stimulation (Fig. 4a), further confirming that the FEME pathway acts as a clathrin-independent endocytic route. However, we found that the different chemical means to inhibit clathrin-mediated endocytosis widely used in the literature (hypertonic shock, K^+ depletion, monodansylcadaverine, chlorpromazine and phenylarsine oxide) all strongly inhibited EPA formation, suggesting pleiotropic effects of these inhibitors

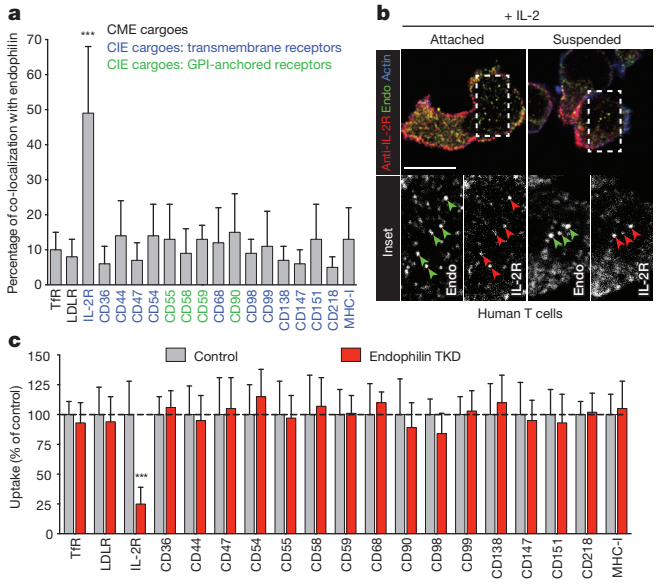

Figure 3 | IL-2R endocytosis by the FEME pathway. **a**, Co-localization of fed antibodies with endogenous endophilin (means ± s.e.m. from three independent experiments; $***P < 0.001$, one-way ANOVA and Dunnett's test versus control IgG). CIE, clathrin-independent endocytosis; CME, clathrin-mediated endocytosis. **b**, Confocal sections of human T cells fixed 10 min after addition of monoclonal anti-IL-2R antibody to the medium and IL-2. Arrowheads indicate EPAs containing internalized IL-2R (images are representatives of at least ten captures from three independent experiments). Scale bar, 5 µm. **c**, Receptor internalization in control or endophilin TKD cells measured with a plate reader (means ± s.e.m. from three independent experiments; $***P < 0.001$, one-way ANOVA and Dunnett's test versus control IgG).

and arguing against their specificity for clathrin-mediated endocytosis. Dynamin is probably the main driver of membrane scission in the FEME pathway, as overexpressing dominant-negative mutants K44A and T65A, depleting its levels by RNAi or inhibiting its function using five different small inhibitors including dynasore and dyngo-4a abrogated EPA budding (Fig. 4a and Extended Data Fig. 8c). Perturbing actin polymerization with cytochalasin D, latrunculin A, jasplakinolide or Arp2/3 inhibitors blocked EPA formation, even at a concentration that did not block clathrin-mediated endocytosis (Fig. 4b and Extended Data Figs 8f, g and 9a). Perturbation of Rho and of Rac blocked the pathway, consistent with their known inhibition of IL-2Rβ uptake[24,27]. Surprisingly, inhibition of Cdc42 increased EPA formation (Fig. 4b, Extended Data Fig. 8f and Supplementary Video 5). All known inhibitors of clathrin-independent endocytosis/macropinocytosis tested also inhibited the FEME pathway (Fig. 4c). However, overexpression of the BAR domain of endophilin lacking its N-terminal amphipathic helix (ΔH0-BAR) was a good inhibitor of the pathway (Fig. 4c, d and Extended Data Fig. 8d, e), suggesting a specific way to inhibit the pathway. It acts by heterodimerizing with endogenous endophilin, and thus decreasing its recruitment to the membrane. Interestingly, many inhibitors acted very promptly (seconds) on endophilin recruitment to the plasma membrane (Extended Data Fig. 8g). Key inhibitors of EPA formation also inhibited FEME cargo uptake but not transferrin uptake and perturbed directed cell migration (Extended Data Fig. 9a, b). Altogether, this established FEME as a clathrin-independent but dynamin-, cholesterol-, actin-, Rac-, Rho-, phosphatidylinositol-3-OH kinase (P(I)3K)- and PAK1-dependent endocytic pathway.

PtdIns(3,4)P_2 is required for FEME

The prominence of endophilin signals at the leading edge of migrating cells (also called the lamellipodium) and its inhibition by class I PI(3)K inhibitors suggested a role for phosphatidylinositol-3,4,5-triphosphate (PtdIns(3,4,5)P_3), as it is produced from the phosphorylation of phosphatidylinositol-4,5-bisphosphate (PtdIns(4,5)P_2) by class I PI(3)K upon receptor activation and is enriched at the leading edge[28,29]. Once generated, PtdIns(3,4,5)P_3 is rapidly hydrolysed back into PtdIns(4,5)P_2 by the 3′-phosphatase PTEN (Fig. 5a and ref. 30). As expected, genetic or chemical inhibition of PTEN significantly increased the recruitment of endophilin at the leading edge in a class I PI(3)K-dependent manner (Fig. 5b, c and Extended Data Fig. 9c). Surprisingly, inhibition of the 5′-phosphatases SHIP1 and SHIP2, that hydrolyse PtdIns(3,4,5)P_3 into PtdIns(3,4)P_2[31], strongly reduced the recruitment of endophilin at the leading edge (Fig. 5b, c and Extended Data Fig. 9c). As both the levels of PtdIns(3,4,5)P_3 and PtdIns(3,4)P_2 were elevated in PTEN-inhibited cells (ref. 32 and Extended Data Fig. 9e), but only those of PtdIns(3,4)P_2 were decreased in SHIP1 plus SHIP2-depleted cells, it indicated that PtdIns(3,4)P_2 was required for the recruitment of endophilin. This was confirmed by the unusual recruitment of endophilin onto endosomes/lysosomes in cells depleted for the 4′-phosphatases INPP4A and INPP4B (Extended Data Fig. 9f). INPP4A and INPP4B dephosphorylate PtdIns(3,4)P_2 into PtdIns(3)P at endosomes[33]. We further established that PtdIns(3,4)P_2 produced from PtdIns(4)P by the class II PI(3)K C2α (which is insensitive to class I PI(3)K inhibitors) was not involved in endophilin recruitment at the leading edge (Fig. 5b, c and Extended Data Fig. 9c), consistent with the recruitment of this kinase to clathrin-coated pits[34]. Thus, we concluded that the formation of

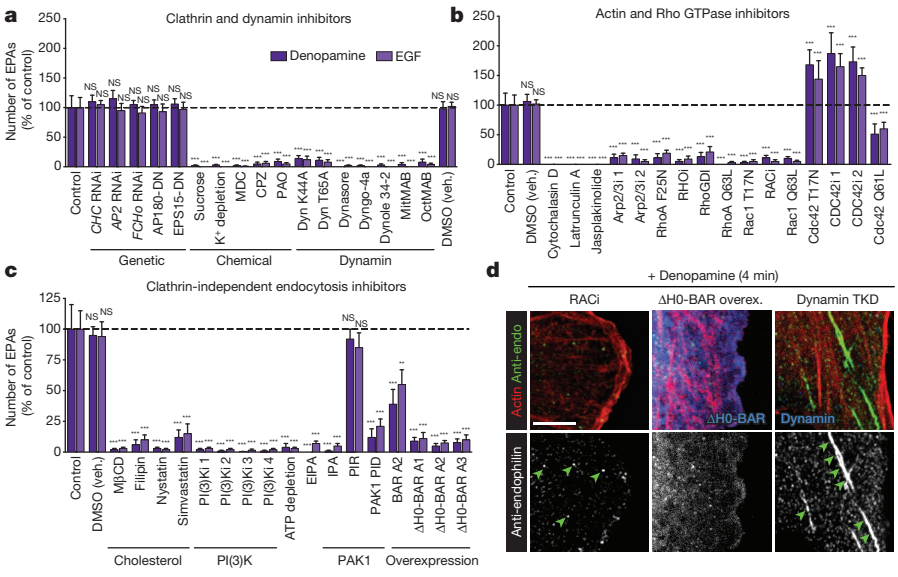

Figure 4 | Regulation of the FEME endocytic pathway. **a–c**, Quantification of the number of EPAs in cells pre-treated with the indicated genetic or chemical clathrin-mediated endocytosis and dynamin inhibitors (CPZ, chlorpromazine; MDC, monodansylcadaverine; PAO, phenylarsine oxide) (**a**), actin/Rho GTPase inhibitors (**b**) or clathrin-independent endocytosis inhibitors (EIPA, 5-(*N*-ethyl-*N*-isopropyl) amiloride; IPA, IPA-3; MβCD, methyl-β-cyclodextrin; PIR, PIR 3.5) (**c**) before stimulation with denopamine or EGF (means ± s.e.m. from three independent experiments; NS, non-significant; $**P < 0.01$; $***P < 0.001$, one-way ANOVA and Dunnett's test versus control). **d**, Confocal sections of cells depleted for dynamin 1, 2 and 3 (TKD), overexpressing high levels of ΔH0-EndoBAR or treated with the EHT1864 (RACi) for 5 min before stimulation with denopamine, fixed and immunostained for endogenous endophilin and actin (images are representatives of at least ten captures). Scale bar, 5 µm.

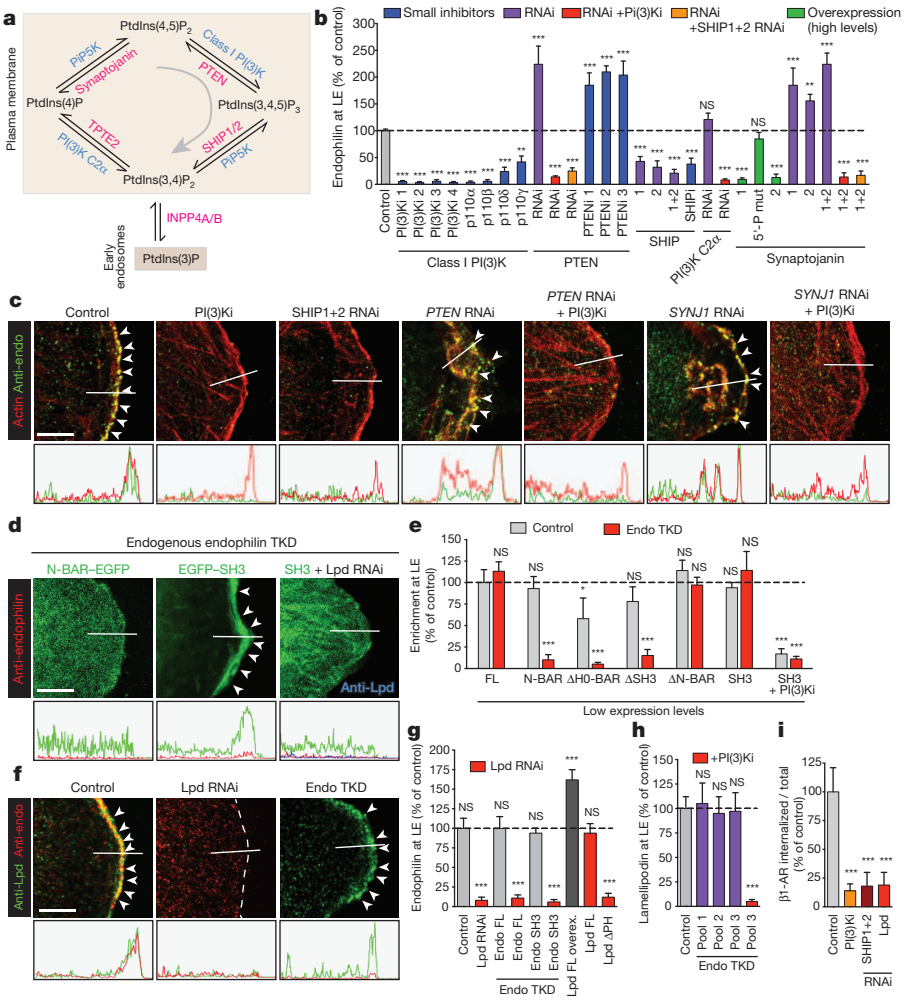

Figure 5 | PtdIns(3,4)P_2 recruits lamellipodin, which in turn engages endophilin at leading edges of cells. **a**, Pathways of phosphoinositide formation by kinases (turquoise) and hydrolysis by phosphatases (pink). **b**, Quantification of levels of endogenous endophilin at the leading edges (LE) of cells treated with the indicated small inhibitors (blue), RNAi (purple), RNAi plus class I PI(3)K inhibitor (red), RNAi + SHIP1+2 RNAi (orange) or cells overexpressing high levels of constructs (green) (means ± s.e.m. from three independent experiments; NS, non-significant; $^{**}P < 0.01$; $^{***}P < 0.001$, one-way ANOVA and Dunnett's test versus control). **c**, Confocal images of endogenous endophilin (green) and actin (red) in cells treated for the indicated RNAi and incubated or not with a specific class I PI(3)K inhibitor (images are representatives of at least ten captures). Intensity profiles were acquired along the indicated lines. **d**, Confocal sections of endophilin TKD cells expressing low levels of the indicated constructs. Endophilin (red) and lamellipodin (blue, right) were counterstained to control for protein depletion in the cells imaged (images are representatives of 10 captures). Intensity profiles were acquired along the indicated lines. **e**, **g**, **h**, Quantification of construct (**e**), endogenous endophilin (**g**) or lamellipodin (**h**) levels at leading edge of cells treated as indicated (means ± s.e.m. from three independent experiments; NS, non-significant; $^{*}P < 0.05$; $^{***}P < 0.001$, one-way ANOVA and Dunnett's test versus control). **f**, Confocal sections of cells treated as indicated and immunostained for endophilin (red) and lamellipodin (green) (images are representatives of ten captures). **i**, β_1-AR uptake in cells treated with the indicated inhibitor or siRNA (means ± s.e.m. from three independent experiments; $^{***}P < 0.001$, one-way ANOVA and Dunnett's test versus control). Scale bars, 5 μm.

PtdIns(3,4,5)P_3 followed by its subsequent dephosphorylation into PtdIns(3,4)P_2 mediate the recruitment of endophilin at the leading edge.

The 5′-phosphatases synaptojanin 1 and 2 dephosphorylate PtdIns(4,5)P_2 into PtdIns(4)P and bind to endophilin[1,19]. Overexpression of synaptojanin repressed endophilin levels at the leading edge and depletion enhanced it (Fig. 5b, c and Extended Data Fig. 9c, d). As all of PtdIns(4,5)P_2, PtdIns(3,4,5)P_3 and PtdIns(3,4)P_2 were increased in synaptojanin 1 and synaptojanin 2 depleted cells (Extended Data Fig. 9e), and as the increased recruitment of endophilin at the leading edge in these cells was class I PI(3)K- and SHIP1/2-dependent, we concluded that synaptojanin acts as a negative regulator for endophilin recruitment by regulating the levels of PtdIns(4,5)P_2, the precursor of the lipid cascade mediating its recruitment at the leading edge of cells. These observations do not preclude a role for synaptojanin in uncoating endophilin from EPAs.

Lamellipodin recruits endophilin at leading edge

The requirement for PtdIns(3,4)P_2 in the recruitment of endophilin to the leading edge could not be explained by the lipid specificity of its N-BAR (containing N-terminal amphipathic helices) domain *in vitro*[35]. Thus, we performed a domain function analysis to understand what part of endophilin was required for its targeting to the leading edge. When overexpressed in cells the N-BAR domains of endophilin-A1, endophilin-A2 and endophilin-A3 are recruited at the leading edge (Extended Data Fig. 10a–d), but as ectopic BAR domains heterodimerize with endogenous endophilin (Extended Data Fig. 8d), it was important to test their targeting in cells depleted for endogenous endophilin. Notably, the N-BAR domain was plasma-membrane-localized in these cells but no longer targeted the leading edge (Fig. 5d, e and Extended Data Fig. 10a–d). We further established that the SH3 domain was necessary and sufficient for the targeting of the constructs in endophilin TKD cells. The recruitment of the SH3 domain was class I PI(3)K- and SHIP1/2-dependent, and as there is, to our knowledge, no evidence in the literature for lipid binding by SH3 domains, we hypothesized that a PtdIns(3,4)P_2-binding protein was recruiting endophilin.

Lamellipodin is the only known endophilin interactor that binds to PtdIns(3,4)P_2 (refs 36, 37). Depleting cells of lamellipodin was sufficient to abrogate the recruitment of overexpressed SH3 domains in endophilin TKD cells as well as endogenous endophilin in control cells, even upon EGF simulation (Fig. 5f, g and Extended Data Fig. 10e–h). Consistently, overexpressing lamellipodin increased endophilin recruitment. Importantly, lamellipodin was still targeted at the leading edge in endophilin TKD cells (Fig. 5f, h), confirming that lamellipodin was upstream of endophilin and was recruiting it, not the other way around. As expected[36], the recruitment of lamellipodin to the leading edge was class I PI(3)K- and SHIP1/2-dependent (thus PtdIns(3,4)P_2-dependent) and required its PH domain (Fig. 5g and Extended Data Fig. 10h, i). Therefore, lamellipodin is the protein that senses PtdIns(3,4)P_2 and recruits endophilin at the leading edge of cells, both processes being required for β_1-AR uptake (Fig. 5i) and thus FEME carrier formation.

Discussion

Endophilin has been associated with clathrin-mediated endocytosis, but recent studies suggested that this view may need to be broadened[15,38]. We present evidence that endophilin functions at the nexus of a clathrin-independent, dynamin-dependent pathway of endocytosis, operating

from distinct regions of the cells, on a different timescale to clathrin-mediated endocytosis (Extended Data Fig. 10j). We define the FEME pathway as the rapid formation (seconds in our cells) at the cell surface of tubulo-vesicular (<1 μm) carriers, positive for endophilin, that rapidly travel towards the cell centre promptly after stimulation of cargo receptors by their cognate ligands. Possibly, this will be extended to the growth cones and synapses in neurons where fast clathrin-independent endocytosis was reported[14,15,39].

Building an endocytic vesicle requires cargo recruitment adaptors, membrane curvature effectors and a membrane scission machinery[40]. Endophilin has all these characteristics in one protein, thus explaining its central role in FEME carrier formation. Its SH3 domain binds to cargo receptors, its BAR domain induces membrane curvature, and by insertion of its multiple amphipathic helices, can support membrane scission[41], aided by the recruitment of dynamin[13]. We show that, mechanistically, receptors need to be activated to become FEME cargoes, and that PtdIns(3,4)P_2, produced from the dephosphorylation of PtdIns(3,4,5)P_3 by SHIP phosphatases, mediates the engagement of lamellipodin, which in turn recruits endophilin at the plasma membrane.

The FEME pathway mediates the cellular entry of the well-established clathrin-independent cargoes[24,42,43] cholera and shiga toxins (see accompanying paper[44]) and IL-2R but not of the other cargoes tested. The variety of receptors entering by the FEME pathway suggests a role in many cellular functions and presents ample opportunity for viruses and other pathogens to exploit the pathway.

Online Content Methods, along with any additional Extended Data display items and Source Data, are available in the online version of the paper; references unique to these sections appear only in the online paper.

Received 15 August; accepted 17 November 2014.
Published online 17 December 2014.

1. Ringstad, N., Nemoto, Y. & De Camilli, P. The SH3p4/Sh3p8/SH3p13 protein family: binding partners for synaptojanin and dynamin via a Grb2-like Src homology 3 domain. *Proc. Natl Acad. Sci. USA* **94,** 8569–8574 (1997).
2. Guichet, A. *et al.* Essential role of endophilin A in synaptic vesicle budding at the *Drosophila* neuromuscular junction. *EMBO J.* **21,** 1661–1672 (2002).
3. Verstreken, P. *et al.* Endophilin mutations block clathrin-mediated endocytosis but not neurotransmitter release. *Cell* **109,** 101–112 (2002).
4. Schuske, K. R. *et al.* Endophilin is required for synaptic vesicle endocytosis by localizing synaptojanin. *Neuron* **40,** 749–762 (2003).
5. Milosevic, I. *et al.* Recruitment of endophilin to clathrin-coated pit necks is required for efficient vesicle uncoating after fission. *Neuron* **72,** 587–601 (2011).
6. Ringstad, N. *et al.* Endophilin/SH3p4 is required for the transition from early to late stages in clathrin-mediated synaptic vesicle endocytosis. *Neuron* **24,** 143–154 (1999).
7. Gad, H. *et al.* Fission and uncoating of synaptic clathrin-coated vesicles are perturbed by disruption of interactions with the SH3 domain of endophilin. *Neuron* **27,** 301–312 (2000).
8. Andersson, F., Low, P. & Brodin, L. Selective perturbation of the BAR domain of endophilin impairs synaptic vesicle endocytosis. *Synapse* **64,** 556–560 (2010).
9. Sundborger, A. *et al.* An endophilin-dynamin complex promotes budding of clathrin-coated vesicles during synaptic vesicle recycling. *J. Cell Sci.* **124,** 133–143 (2011).
10. Perera, R. M., Zoncu, R., Lucast, L., De Camilli, P. & Toomre, D. Two synaptojanin 1 isoforms are recruited to clathrin-coated pits at different stages. *Proc. Natl Acad. Sci. USA* **103,** 19332–19337 (2006).
11. Ferguson, S. M. *et al.* Coordinated actions of actin and BAR proteins upstream of dynamin at endocytic clathrin-coated pits. *Dev. Cell* **17,** 811–822 (2009).
12. Taylor, M. J., Perrais, D. & Merrifield, C. J. A high precision survey of the molecular dynamics of mammalian clathrin-mediated endocytosis. *PLoS Biol.* **9,** e1000604 (2011).
13. Meinecke, M. *et al.* Cooperative recruitment of dynamin and BIN/amphiphysin/Rvs (BAR) domain-containing proteins leads to GTP-dependent membrane scission. *J. Biol. Chem.* **288,** 6651–6661 (2013).
14. Jockusch, W. J., Praefcke, G. J., McMahon, H. T. & Lagnado, L. Clathrin-dependent and clathrin-independent retrieval of synaptic vesicles in retinal bipolar cells. *Neuron* **46,** 869–878 (2005).
15. Llobet, A. *et al.* Endophilin drives the fast mode of vesicle retrieval in a ribbon synapse. *J. Neurosci.* **31,** 8512–8519 (2011).
16. Tang, Y. *et al.* Identification of the endophilins (SH3p4/p8/p13) as novel binding partners for the beta1-adrenergic receptor. *Proc. Natl Acad. Sci. USA* **96,** 12559–12564 (1999).
17. Petrelli, A. *et al.* The endophilin-CIN85-Cbl complex mediates ligand-dependent downregulation of c-Met. *Nature* **416,** 187–190 (2002).
18. Soubeyran, P., Kowanetz, K., Szymkiewicz, I., Langdon, W. Y. & Dikic, I. Cbl-CIN85-endophilin complex mediates ligand-induced downregulation of EGF receptors. *Nature* **416,** 183–187 (2002).
19. Cremona, O. *et al.* Essential role of phosphoinositide metabolism in synaptic vesicle recycling. *Cell* **99,** 179–188 (1999).
20. Parton, R. G. & del Pozo, M. A. Caveolae as plasma membrane sensors, protectors and organizers. *Nature Rev. Mol. Cell Biol.* **14,** 98–112 (2013).
21. Glebov, O. O., Bright, N. A. & Nichols, B. J. Flotillin-1 defines a clathrin-independent endocytic pathway in mammalian cells. *Nature Cell Biol.* **8,** 46–54 (2006).
22. Lundmark, R. *et al.* The GTPase-activating protein GRAF1 regulates the CLIC/GEEC endocytic pathway. *Curr. Biol.* **18,** 1802–1808 (2008).
23. Sigismund, S. *et al.* Clathrin-mediated internalization is essential for sustained EGFR signaling but dispensable for degradation. *Dev. Cell* **15,** 209–219 (2008).
24. Lamaze, C. *et al.* Interleukin 2 receptors and detergent-resistant membrane domains define a clathrin-independent endocytic pathway. *Mol. Cell* **7,** 661–671 (2001).
25. Sauvonnet, N., Dujeancourt, A. & Dautry-Varsat, A. Cortactin and dynamin are required for the clathrin-independent endocytosis of gammac cytokine receptor. *J. Cell Biol.* **168,** 155–163 (2005).
26. Maldonado-Báez, L., Williamson, C. & Donaldson, J. G. Clathrin-independent endocytosis: a cargo-centric view. *Exp. Cell Res.* **319,** 2759–2769 (2013).
27. Grassart, A., Dujeancourt, A., Lazarow, P. B., Dautry-Varsat, A. & Sauvonnet, N. Clathrin-independent endocytosis used by the IL-2 receptor is regulated by Rac1, Pak1 and Pak2. *EMBO Rep.* **9,** 356–362 (2008).
28. Fritsch, R. & Downward, J. SnapShot: Class I PI3K isoform signaling. *Cell* **154,** 940 (2013).
29. Servant, G. *et al.* Polarization of chemoattractant receptor signaling during neutrophil chemotaxis. *Science* **287,** 1037–1040 (2000).
30. Song, M. S., Salmena, L. & Pandolfi, P. P. The functions and regulation of the PTEN tumour suppressor. *Nature Rev. Mol. Cell Biol.* **13,** 283–296 (2012).
31. Xie, J., Erneux, C. & Pirson, I. How does SHIP1/2 balance PtdIns(3,4)P_2 and does it signal independently of its phosphatase activity? *Bioessays* **35,** 733–743 (2013).
32. Batty, I. H. *et al.* The control of phosphatidylinositol 3,4-bisphosphate concentrations by activation of the Src homology 2 domain containing inositol polyphosphate 5-phosphatase 2, SHIP2. *Biochem. J.* **407,** 255–266 (2007).
33. Gewinner, C. *et al.* Evidence that inositol polyphosphate 4-phosphatase type II is a tumor suppressor that inhibits PI3K signaling. *Cancer Cell* **16,** 115–125 (2009).
34. Posor, Y. *et al.* Spatiotemporal control of endocytosis by phosphatidylinositol-3,4-bisphosphate. *Nature* **499,** 233–237 (2013).
35. Yoon, Y., Zhang, X. & Cho, W. Phosphatidylinositol 4,5-bisphosphate (PtdIns(4,5)P_2) specifically induces membrane penetration and deformation by Bin/amphiphysin/Rvs (BAR) domains. *J. Biol. Chem.* **287,** 34078–34090 (2012).
36. Krause, M. *et al.* Lamellipodin, an Ena/VASP ligand, is implicated in the regulation of lamellipodial dynamics. *Dev. Cell* **7,** 571–583 (2004).
37. Vehlow, A. *et al.* Endophilin, Lamellipodin, and Mena cooperate to regulate F-actin-dependent EGF-receptor endocytosis. *EMBO J.* **32,** 2722–2734 (2013).
38. Kononenko, N. L. *et al.* Clathrin/AP-2 mediate synaptic vesicle reformation from endosome-like vacuoles but are not essential for membrane retrieval at central synapses. *Neuron* **82,** 981–988 (2014).
39. Watanabe, S. *et al.* Ultrafast endocytosis at mouse hippocampal synapses. *Nature* **504,** 242–247 (2013).
40. McMahon, H. T. & Boucrot, E. Molecular mechanism and physiological functions of clathrin-mediated endocytosis. *Nature Rev. Mol. Cell Biol.* **12,** 517–533 (2011).
41. Boucrot, E. *et al.* Membrane fission is promoted by insertion of amphipathic helices and is restricted by crescent BAR domains. *Cell* **149,** 124–136 (2012).
42. Römer, W. *et al.* Shiga toxin induces tubular membrane invaginations for its uptake into cells. *Nature* **450,** 670–675 (2007).
43. Ewers, H. *et al.* GM1 structure determines SV40-induced membrane invagination and infection. *Nature Cell Biol.* **12,** 11–18 (2010).
44. Renard, H.-F. *et al.* Endophilin-A2 functions in membrane scission in clathrin-independent endocytosis. *Nature* http://dx.doi.org/10.1038/nature14064 (2014).

Supplementary Information is available in the online version of the paper.

Acknowledgements We thank S. Y. Peak-Chew for mass spectrometry, M. Edwards and K. McGourty for technical help and P. De Camilli, T. Kirchhausen, G. B. Hammond, P. Robinson, M. Robinson, M. McNiven, B. Nichols, A. Benmerah, M. Krause and Genentech for the gift of reagents, and the members of the McMahon and Boucrot laboratories for comments. The research was funded by the Medical Research Council UK (grant number U105178805) (H.T.M., L.A.-S., G.H., Y.V. and E.B. in part) and a Royal Society grant (research grant number RG120481) (E.B.). A.P.A.F is supported by the Fundação para a Ciência e Tecnologia, L.A.-S. is a EMBO Long Term fellow and is supported by Marie Curie Actions, and E.B. is a Biotechnology and Biological Sciences Research Council (BBSRC) David Phillips Research Fellow.

Author Contributions H.T.M. and E.B. designed the research and supervised the project. H.T.M. and A.P.A.F. performed pull-down experiments. L.A.-S., A.P.A.F. and S.D. did the signalling experiments. L.A.-S. did the super-resolution imaging. A.P.A.F. did the cell migration experiments. S.D. performed the plasma membrane isolations; Y.V. performed the PC12 cell experiments. G.H. prepared and acquired the electron-microscopy data. L.B. and N.S. provided critical reagents. E.B. performed and analysed all the other experiments. E.B. and H.T.M. wrote the manuscript with input from all the other authors.

Author Information Reprints and permissions information is available at www.nature.com/reprints. The authors declare no competing financial interests. Readers are welcome to comment on the online version of the paper. Correspondence and requests for materials should be addressed to H.T.M. (hmm@mrc-lmb.cam.ac.uk) or E.B. (e.boucrot@ucl.ac.uk).

METHODS

Cell culture. BSC1 (ECACC 85011422) and HEK293 cells (ATCC CRL-1573) were cultured in DMEM (Sigma) supplemented with 10% fetal bovine serum (FBS, Gold PAA), 1 mM GlutaMAX-I (Gibco). Normal human epithelial cells hTERT-RPE1 (ATCC CRL-4000) were cultured in DMEM:F12 HAM (1:1 v/v) (Sigma), 0.25% sodium bicarbonate (w/v) (Sigma), 1 mM GlutaMAX-I (Gibco) and 10% FBS (Gold, PAA). Human dermal primary fibroblasts from adult donors (hDFA; ATCC PCS-201-012) were maintained in DMEM:F12 HAM (1:1 v/v) (Sigma), 2% FBS, 1 mM GlutaMAX-I, 0.8 μM insulin, 1 μg ml^{-1} hydrocortisone, 50 μg ml^{-1} ascorbic acid (Sigma) and 5 ng ml^{-1} bFGF (R&D). hDFA were used within 15–20 population doublings *in vitro* to ensure a minimum percentage of senescent cells within the cell population. Human T cells Kit255 (expressing endogenous IL-2R) were cultured in RPMI 1640 (Sigma) supplemented with 10% FBS, 1 mM GlutaMAX-I and 200 pM IL-2. Rat PC12 neuroendocrine cells were cultured in RPMI 1640 supplemented with 7.5% FBS and 7.5% heat inactivated horse serum and 1 mM GlutaMAX-I. BSC1 cells stably expressing σ2-EGFP were a gift from T. Kirchhausen (Harvard Medical School, USA) and were cultured as parental BSC1 cells with the additional of 200 μg ml^{-1} G418. Approximately 2×10^6, 2×10^5, 2.5×10^4 or 5×10^3 cells were seeded on 100 mm, 35 mm dishes, 13 mm coverslips or 96-well glass bottom plates, respectively. Cells were regularly tested for mycoplasma contamination.

Gene cloning. N-BAR, Δhelix0 BAR, ΔSH3, ΔN-BAR, SH3 domains or full-length endophilin-A1 (*SH3GL2*, FLJ 92732), -A2 (*SH3GL1*, IMAGE 3458016) and -A3 iso 1 (*SH3GL3*, IMAGE 5197246) genes were cloned into pDONR201 (Invitrogen) and transferred into pEGFP, pTagRFP-T[45] (called 'RFP' elsewhere), pTagBFP (called 'BFP' elsewhere) or pGEX-6P2 vectors converted into the Gateway system (pDEST vectors). Mouse β_1 adrenergic receptor (*ADRB1*, IMAGE 9055582) full length, third intracellular loop (TIL, amino acids (aa) 246–315) and C terminus (C-term, aa 370–end), human β_2 adrenergic receptor (*ADRB2*, IMAGE 5217922) full length, TIL (aa 220–274) and C-term (aa 330–end), human β_3 adrenergic receptor (*ADRB3*, IMAGE 30915407) TIL (aa 225–294) and C-term (aa 350–end), human α_{2a} adrenergic receptor (*ADRA2A*, IMAGE 6198830) full length, TIL (aa 218–374), human α_{2b} adrenergic receptor (*ADRA2B*, IMAGE 9020527) full length, TIL (aa 194–372), human dopamine receptor 1 (*DRD1*, IMAGE 30915297) full length, TIL (aa 219–272) and C-term (aa 338–end), human dopamine receptor 2 (*DRD2*, IMAGE 3939741) full length, human dopamine receptor 3 (*DRD3*, IMAGE 40112299) full length, TIL (aa 210–329), mouse dopamine receptor 4 (*DRD4*, IMAGE 6492837) full length, TIL (aa 309–314), human dopamine receptor 5 (*DRD5*, IMAGE 3928370) full length, TIL (aa 247–296) and C-term (aa 361–end), human serotonin receptor 6 (*HTR6*, IMAGE 30915608) TIL (aa 209–265) and C-term (aa 321–end), human serotonin receptor 7 (*HTR7*, IMAGE 5297325) TIL (aa 258–325) and C-term (aa 389–end), human muscarinic acetylcholine receptor M1 (*CHRM1*, IMAGE 4931283) full length, TIL (aa 210–366), human muscarinic acetylcholine receptor M2 (*CHRM2*, IMAGE 40017105) full length, TIL (aa 208–388), human muscarinic acetylcholine receptor M4 (*CHRM4*, IMAGE 9021535) full length, TIL (aa 217–401), human histamine receptor 1 (*HRH1*, IMAGE 30340368) TIL (aa 211–418) and human histamine receptor 3 (*HRH3*, IMAGE 6971899) TIL (aa 218–359), human CIN85 (*SH3BP1*, IMAGE 3906722) SH3(3) (aa 1–328), PRD (aa 327–428), and PCC (aa 327–end), human Cbl-PRD (aa 477–end), human RhoGDI (*ARHDIA*, IMAGE 4867857), rat β-arrestin 1 and 2 full length, human ALIX (*PDCD6IP*, IMAGE 4340998) PRD domain (aa 717–end) and human PAK1 (*PAK1*, Addgene 23543) PAK1-inhibitory domain PID (aa 89–149) were cloned into pDONR201 and transferred into pEGFP DEST vectors.

Double-tagged HA–β1AR–EGFP, HA–β_2AR–EGFP, HA–α_{2a}AR–EGFP, HA–α_{2b}AR–EGFP, HA–DR1–EGFP, HA–DR2–EGFP, HA–DR3–EGFP, HA–DR4–EGFP, HA–DR5–EGFP, HA–mAchR1–EGFP, HA–mAchR2–EGFP, HA–mAchR4–EGFP plasmids were cloned by inserting a HA tag at the N terminus (thus at the extracellular extremity) into the pDONR201 clones containing full-length receptors described above and then transferred into a pEGFP-C DEST vector. Point mutations β_1-AR R271A, P272/273A, R285A, P283/284A, P272/273/283/284A and R298/299A; DR3 K293E and R318E; DR4 P230/233A, R3236D R237E, R276E; and mAchR4 R230E, K255/256E and P331E were introduced by site-directed mutagenesis in the entry or expression clones containing the TIL of the respective receptors. Alix R757E (ref. 46) was introduced into the PRD clone. Human RhoA F25N, Rac1 T17N, Cdc42 T17N, Rac1 Q61L, RhoA Q63L and Cdc42 Q61L mutants were cloned into pEGFP-expressing vectors. Rat EGFP–LCa (clathrin light chain a) was provided by M. Robinson, rat dynamin 2–EGFP and K44A variant were gifts of M. McNiven, rat EGFP–synaptojanin 1 (145 and 170 isoforms) and Flag–synaptojanin 2 (isoform 1) were gifts of P. De Camilli; synaptojanin 1 D730A (5′-phosphatase mutant[10]) was introduced by quickchange mutagenesis. EGFP–Flotillin-1 was provided by B. Nichols, EGFP–Eps15 Δ95/295 (called 'Eps15-DN' here) was a gift from A. Benmerah and EGFP–lamellipodin was a gift from M. Krause, the ΔPH domain version of lamellipodin was generated by quickchange mutagenesis. GRAF1–EGFP[22], EGFP–AP180 C terminus (residues 530–915, called 'AP180-DN' here)[47], dynamin1 T65A[48] and FCHo2–EGFP[49] have been described earlier.

Gene transfection. For live-cell imaging localization experiments, cells seeded on 35 mm glass bottom dishes (MatTek) were transfected using Lipofectamine 2000 (Invitrogen) or Nanofectin (PAA) and 50–250 ng DNA (the levels of each plasmid were titrated down to levels allowing good detection but limiting side effects of overexpression). For dominant-negative mutants, 1 μg of plasmids were used. For endogenous staining on fixed samples, cells seeded on 13 mm coverslips (placed in 24-well plates) were transfected using Lipofectamine 2000 (Invitrogen) or Nanofectin (PAA) and 0.5–50 ng DNA depending on the plasmids and the experiments (low or high overexpression). For receptor tails extracts, cells seeded on 100 mm dishes were transfected using Nanofectin (PAA) and 1–3 μg DNA. Cells were incubated 24 h to express the constructs and were either imaged live, fixed (3.7% paraformaldehyde, 20 min) or processed to prepare the cell extracts.

siRNA suppression of gene expression. The following siRNA used were: endophilin A1+2+3 pool 1: Invitrogen Stealth HSS109710, HSS109705 and HSS109713 (targeting human *SH3GL2*, *SH3GL1* and *SH3GL3*, respectively); endophilin A1+2+3 pool 2: Invitrogen Stealth HSS109708, HSS109706 and HSS109711 (targeting human *SH3GL2*, *SH3GL1* and *SH3GL3*, respectively); endophilin A1+2+3 pool 3: Invitrogen Stealth HSS109709, HSS109707, HSS109712 (targeting human *SH3GL2*, *SH3GL1* and *SH3GL3*, respectively); endophilin B1 and B2: Dharmacon D-015810-01 and D-015810-02 (targeting human *SH3GLB1* and *SH3GLB2*, respectively); rat EndoA1+2+3 pool (PC12 cell experiments): 3 oligos against A1 (*SH3GL2*) RSS300636, RSS350431 and RSS350432, 3 oligos against A2 (*SH3GL1*) RSS330960, RSS360961 and RSS372917, 3 oligos against A3 (*SH3GL3*) RSS330957, RSS330958 and RSS330959; clathrin heavy chain CHC: Invitrogen Stealth HSS174637; AP2: mu2-2 defined in ref. 50 or Invitrogen Stealth HSS101955 (targeting human *AP2M1*); β-arrestin 1 and 2: Thermo Scientific L-011971 and L-007292 (targeting human *ARRB1* and *ARRB2*, respectively), Cbl: Dharmacon ON-TARGETplus SMARTpool (mix of J-003003-09, J-003003-10, J-003003-11 and J-003003-12 targeting human *CBL*); CIN85: Dharmacon ON-TARGETplus SMARTpool (mix of J-014748-08, J-014748-07, J-014748-06 and J-014748-05 targeting human *SH3KBP1*); dynamin 1: Dharmacon ON-TARGETplus SMARTpool (mix of J-003940-05, J-003940-06, J-003940-07 and J-003940-08 targeting human *DNM1*); dynamin 2: Dharmacon ON-TARGETplus SMARTpool (mix of J-004007-05, J-004007-06, J-004007-07 and J-004007-08 targeting human *DNM2*); dynamin 3: Dharmacon ON-TARGETplus SMARTpool (mix of J-013931-05, J-013931-06, J-013931-07 and J-013931-08 targeting human *DNM3*); lamellipodin: Dharmacon ON-TARGETplus SMARTpool (mix of J-031919-08, J-031919-07, J-031919-06 and J-031919-05 targeting human *RAPH1*); SHIP1: Dharmacon ON-TARGETplus SMARTpool (mix of J-003013-09, J-003013-10, J-003013-11 and J-003013-12 targeting human *INPP5D*); SHIP2: Dharmacon ON-TARGETplus SMARTpool (mix of J-004152-06, J-004152-07, J-004152-08 and J-004152-09 targeting human *INPPL1*); PTEN: Dharmacon ON-TARGETplus SMARTpool (mix of J-003023-09, J-003023-10, J-003023-11 and J-003023-12 targeting human *PTEN*); PI3K-C2α: Dharmacon ON-TARGETplus SMARTpool (mix of J-006771-08, J-006771-07, J-006771-06 and J-006771-05 targeting human *PI3KC2A*); INPP4A: Dharmacon ON-TARGETplus SMARTpool (mix of J-011299-06, J-011299-07, J-011299-08 and J-011299-09 targeting human *INPP4A*); INPP4B: Dharmacon ON-TARGETplus SMARTpool (mix of J-011539-17, J-011539-18, J-011539-19 and J-011539-08 targeting human *INPP4B*); synaptojanin 1: Dharmacon ON-TARGETplus SMARTpool (mix of J-019486-07, J-019486-08, J-019486-09 and J-019486-10 targeting human *SYNJ1*); synaptojanin 2: Dharmacon ON-TARGETplus SMARTpool (mix of J-019486-07, J-019486-08, J-019486-09 and J-019486-10 targeting human *SYNJ2*). Control siRNA used were Dharmacon ON-TARGETplus GAPDH control (D-001830-01-05), Invitrogen Stealth control (scrambled) oligo 138782 or a mixture of Invitrogen Stealth 'high GC' 45-2000 and 'low GC' 45-2002 oligos.

Cells seeded on 35 mm dishes were transfected twice (on day 1 and 2) with Oligofectamine (Invitrogen) complexed with 80 pmol of each indicated siRNA and analysed 3–4 days after the first transfection. Rescue experiments were performed with plasmid DNA transfection of the indicated constructs at the middle of day 3 (when endogenous levels of the targeted proteins were already decreased) and the cells were analysed 16 h later (on day 4). Transfection of siRNA into human T cells Kit255 was performed by electroporation using a Nucleofector 2b (Lonza) and Ingenio (Mirus Bio) cuvettes and electroporation solutions. RNAi knockdown efficiency was verified by western blotting and immunofluorescence counter staining, when antibodies were available. The use of validated pools of siRNA targeting the same genes increased the knock-down efficiency and specificity.

Protein purification and pull-down experiments. GST-tagged constructs were expressed in BL21 *Escherichia coli* (Stratagene). Cells were lysed using an Emulsiflex C3, spun at 140,000*g* for 40 min at 4 °C in a Beckman Ti45 rotor, and the supernatant was bound to glutathione beads for 30 min. The beads were washed extensively with 150 mM NaCl, 20 mM HEPES pH 7.4, 2 mM DTT, 2 mM EDTA, including

2 washes with 500 mM NaCl. GST-proteins were eluted from the GST-sepharose beads with 10 mM glutathione, further purified by Superdex 200 gel filtration, and rebound to a minimal volume of fresh GST-sepharose beads (to achieve saturation) for use in pull downs. HEK293 cells expressing various EGFP-tagged constructs were quickly washed with cold PBS, lysed in ice-cold lysis buffer (150 mM NaCl, 20 mM HEPES, 5 mM DTT, 0.1% Triton X-100 and a protease and phosphatase inhibitor cocktail (Thermo Scientific)), briefly sonicated and spun at 14,000*g* for 10 min. Bead-bound proteins were then exposed to cell lysates for 1 h, pelleted in a cooled bench-top centrifuge, and washed three times in lysis buffer. The final pellet was boiled in sample buffer and run on SDS–PAGE ('input' lanes correspond to 10% of cell extract). The proteins were transferred onto PVDF membrane and immunoblotted using anti-EGFP antibodies.

Antibodies. The following antibodies were used for immunostaining, flow cytometry or immunoblotting: pan anti-endophilin Ra74 (in-house affinity purified rabbit polyclonal raised against the SH3 domain of rat endophilin A1[15]), anti-endophilin A2 clones H-60 and A-11 (rabbit polyclonal sc-25495 and mouse monoclonal sc-365704, respectively, Santa Cruz Biotechnology), anti-EGFR antibody clone D38B1 used for total staining (rabbit polyclonal, Cell Signaling Technologies 4267), anti-α-adaptin clone 8 (mouse monoclonal, BD Bioscience 610501) and clone AP6 (mouse monoclonal, Thermo Scientific MA1-064), anti-clathrin heavy chain X22 (Thermo Scientific MA1-065), anti-vinculin clone hVIN-1 (mouse monoclonal, Sigma V9264), anti-Arp3 (rabbit polyclonal, Millipore 07-277), anti-cortactin p80/85 clone 4F11 (mouse monoclonal, Millipore 05-180), anti-dynamin clone 41 (mouse monoclonal, BD Transduction Laboratories 610245), anti-caveolin-1 (mouse monoclonal, BD Transduction Laboratories 610059), anti-lamellipodin (mouse monoclonal clone H-5, Santa Cruz sc-390050 and rabbit polyclonal Atlas Antibodies HPA020027), anti-SHIP1 clone D1163 (rabbit polyclonal, Cell Signaling Technologies 2728), anti-SHIP2 clone C76A7 (rabbit polyclonal, Cell Signaling Technologies 2839), anti-synaptojanin (rabbit polyclonal, Abcam 84309), anti-LAMP-1 clone H4A3 (Developmental Studies Hybridoma Bank), anti-calnexin H60 (rabbit polyclonal, Santa Cruz Biotechnology sc-11397), anti-integrin β1 (rabbit polyclonal, Cell Signaling Technologies 4706), anti-β_1-AR (rabbit polyclonal, Cell Signaling Technologies 12271), anti-β-arrestin1/2 (goat polyclonal, Abcam 31294), anti-phosphorylated p44/42 MAPK T202/Y204 (phosphorylated Erk1/2) clone D13.14.4E (rabbit polyclonal, Cell Signaling Technologies 4370), anti-p44/42 MAPK (total Erk1/2) (rabbit polyclonal, Cell Signaling Technologies 9102), anti-phosphorylated Elk1 (Ser 383) (rabbit polyclonal, Cell Signaling Technologies 9181), anti-phosphorylated cJun (Ser 73) clone D47G9 (rabbit polyclonal, Cell Signaling Technologies 3270), anti-phosphorylated CREB (Ser 133) clone 87G3 (rabbit polyclonal, Cell Signaling Technologies 9198), anti-PtdIns(3,4)P_2 (mouse monoclonal, Echelon Bioscience Z-P034b), anti-PtdIns(4,5)P_2 (mouse monoclonal, Echelon Bioscience Z-A045), anti-PtdIns(3,4,5)P_3 (mouse monoclonal, Echelon Bioscience Z-P345b), anti-β-tubulin clone 9F3 (mouse monoclonal, Cell Signaling Technologies 2128), anti-EGFP ab290 (rabbit polyclonal, AbCam 290), anti-Myc tag clone 9E10 (mouse monoclonal, AbGent AM1007a) and clone 9B11 (mouse monoclonal, Cell Signaling Technologies 2276), anti-Flag tag clone M2 (mouse monoclonal, Sigma F1804 and rabbit polyclonal Cell Signaling Technologies 2368), anti-GAPDH clone 0411 (mouse monoclonal, Santa Cruz Biotechnology sc-47724) and clone 14C10 (rabbit polyclonal, Cell Signaling Technologies 2118).

The following antibodies were used for receptor uptake assays ('antibody feeding assays'): anti-HA clone 16B12 used for 'HA–GPCR–EGFP' chimaera uptake assays (mouse monoclonal Covance), anti-EGFR antibody clone 13A9 (mouse monoclonal raised against the ectodomain of EGFR that does not compete with EGF binding, a gift from Genentech), anti-IL-2R clone 561 (mouse monoclonal, recognizing the extracellular portion of IL-2R but does not compete with IL-2 (ref. 51)), anti-NGFR antibody clone 165131 (mouse monoclonal raised against the ectodomain of TrkA, R&D systems MAB2148), anti-TfR clone CBL47 (rabbit polyclonal, Millipore CBL47), anti-LDLR (mouse monoclonal, R&D systems MAB2148), anti-CD36 clone 5-271 (mouse monoclonal, BioLegend 336202), anti-CD44 clone BJ18 (mouse monoclonal, BioLegend 338802), anti-CD47 clone CC2C6 (mouse monoclonal, BioLegend 323102), anti-CD54 (also called ICAM-1) clone HA58 (mouse monoclonal, BioLegend 353101), anti-CD55 clone JS11 (mouse monoclonal, BioLegend 311302), anti-CD58 clone LFA-3 (mouse monoclonal, BioLegend 330902), anti-CD59 clone H19 (mouse monoclonal, BioLegend 304702), anti-CD68 clone Y/82A (mouse monoclonal, BioLegend 333801), anti-CD90 (Thy1) clone IBL-6/23 (rat monoclonal, AbCam ab3105), anti-CD98 clone MEM-108 (mouse monoclonal, BioLegend 315602), anti-CD99 clone TU12 (mouse monoclonal, BD Pharmigen 555687), anti-CD138 clone MI15 (mouse monoclonal, BioLegend 356501), anti-CD147 clone HIM6 (mouse monoclonal, BioLegend 306202), anti-CD151 (mouse monoclonal, ABD Serotec MCA1856T), anti-CD218a clone H44 (mouse monoclonal, BioLegend 313804) and anti-MHC-I HLA-A,B,C clone W6/32 (mouse monoclonal, BioLegend 311402).

Primary antibodies were used at 0.2–5 μg ml^{-1} for immunoblotting, 0.1–10 μg ml^{-1} for immunofluorescence and 10 μg ml^{-1} for antibody feeding assays. Before immunostaining, fixed cells were permeabilized with 0.05% saponin, apart from staining of activated transcription factors (CREB, Elk1 and Jun) which was done after permeabilization with 0.1% Triton X-100 and for phosphoinositide staining which was done as described below.

The following secondary antibodies were used: Alexa Fluor 488 and Alexa Fluor 555 goat anti-mouse IgG, Alexa Fluor 488 and Alexa Fluor 555 goat anti-rabbit IgG, Alexa Fluor 488 goat anti-rat IgG, Alexa Fluor 488 donkey anti-goat IgG and Alexa Fluor 555 donkey anti-rabbit (all from Life Technologies) and goat anti-mouse IgG-HRP conjugate and goat anti-rabbit IgG-HRP conjugate (both from Bio-Rad).

Chemicals, growth factors and small inhibitors. Pre-treatments with small inhibitors before stimulation were performed for 5 min at 37 °C, unless specified otherwise, and the inhibitors were kept during the stimulation or assay periods in all cases. Cytochalasin D (actin depolymerizer, Tocris 1233, used at 100 nM), latrunculin A (actin depolymerizer, Tocris 3973, used at 200 nM), jasplakinolide (actin stabilizer, Tocris 2792, used at 100 nM), rhosin (RhoA inhibitor called 'RHOi' in this study, Calbiochem 555460, used at 10 μM), EHT1864 (RAC inhibitor, called 'RACi 1' in this study, Tocris 3872, used at 2 μM), EHop-016 (RAC inhibitor, called 'RACi 2' in this study, Sigma SML0526, used at 2 μM), secramine[52] (Cdc42 inhibitor, called 'CDC42i 1' in this study, a gift from T. Kirchhausen (Harvard Medical School) and the Hammond lab (Univ. of Louisville) was synthetized by B. Xu and G. B. Hammond, and was used at 10 μM), ML141 (Cdc42 allosteric inhibitor, called 'CDC42i 2' in this study, Tocris 4266, used at 10 μM), CK548 (Arp2/3 inhibitor, called 'Arp2/3i 1' in this study, Sigma C7499, used at 50 μM), CK636 (Arp2/3 inhibitor, called 'Arp2/3i 2' in this study, Sigma C7374, used at 50 μM), methyl-β-cyclodextrin (extracts cholesterol, called 'MßCD' in this study, Sigma 332615, used at 50 μM for three incubations of 10 min each), filipin (sequesters cholesterol, Sigma F4767, used at 1 μg ml^{-1}), nystatin (sequesters cholesterol, Sigma N3503, used at 10 μg ml^{-1}), simvastatin (sequesters cholesterol, Sigma S6196, used at 10 μM), dynasore (dynamin inhibitor[53], a gift of T. Kirchhausen (Harvard Medical School) and used at 80 μM), Dyngo-4a (dynamin inhibitor[54], a gift of P. Robinson (Univ. of Sydney) and used at 20 μM), dynole 34-2 (dynamin inhibitor[55], Tocris 4222, used at 20 μM), MitMAB (dynamin inhibitor[56], Calbiochem 324411, used at 20 μM), OctMAB (dynamin inhibitor[56], Tocris 4225, used at 20 μM), monodansylcadaverine (clathrin-mediated endocytosis inhibitor[57], called 'MDC' in this study, Sigma D4008, used at 100 μM), chlorpromazine (clathrin-mediated endocytosis inhibitor[58], called 'CPZ' in this study, Sigma C8138, used at 10 μg ml^{-1}), phenylarsine oxide PAO (clathrin-mediated endocytosis inhibitor[59], Sigma P3075, used at 10 μM), GDC-0941 (broad and specific PI(3)K inhibitor, called 'PI(3)Ki 1' or 'PI(3)Ki' in this study, Symansis SYGDC0941, used at 50 nM), GSK2126458 (broad and specific PI(3)K inhibitor, called 'PI(3)Ki 2' in this study, BioVision 1961, used at 25 nM), LY294002 (broad PI(3)K inhibitor, called 'PI(3)Ki 3′ in this study, Tocris 1130, used at 50 μM), wortmannin (broad PI(3)K inhibitor, called 'PI(3)Ki 4' in this study, Cell Signaling Technologies 9951, used at 500 nM), A66 S (PI(3)K p110α specific inhibitor, Selleckchem S2636, used at 50 nM), TGX-221 (PI(3)K p110β specific inhibitor, Cayman 10007349, used at 25 nM), CAL-101 (PI(3)K p110δ specific inhibitor, Selleckchem S2226, used at 50 nM), AS-252424 (PI(3)K p110γ specific inhibitor, Cayman 10009052, used at 100 nM), 5-(*N*-ethyl-*N*-isopropyl) amiloride (macropinocytosis inhibitor, called 'EIPA' in this study, Sigma A3085, used at 25 μM), PF-3758309 (broad PAK inhibitor, called 'PAKi' in this study, Calbiochem 500613, used at 1 μM), IPA-3 (PAK1 inhibitor, called 'IPA' in this study, Sigma I2285, used at 20 μM) and PIR 3.5 (IPA-3 inactive analogue, called 'PIR' in this study, Tocris 4212, used at 20 μM), AS 19499490 (SHIP2 inhibitor, called 'SHIP2i' in this study, Tocris 3718, used at 1 μM), bpV(Hopic) (protein tyrosine phosphatase inhibitor with selectivity for PTEN (IC_{50} = 14 nM), called 'PTENi 1' in this study, Cayman 14433, used at 200 nM), bpV(Phen) (protein tyrosine phosphatase inhibitor with selectivity for PTEN (IC_{50} = 38 nM), called 'PTENi 2' in this study, Santa Cruz Biotechnology sc-221378, used at 200 nM), SF1670 (PTEN inhibitor, called 'PTENi 3' in this study, Cayman 15368, used at 10 μM), PD153035 (EGFR inhibitor, called 'EGFRi' in this study, Tocris 1037, used at 5 μM), SB590885 (RAF inhibitor, called 'RAFi' in this study, Tocris 2650, used at 5 μM), PD032591 (MEK inhibitor, called 'MEKi 1' in this study, Tocris 4192, used at 0.5 mM), U0126 (MEK inhibitor, called 'MEKi 2' in this study, Cell Signaling Technologies 99035, used at 10 mM). Sucrose hypertonic treatment (inhibiting clathrin-mediated endocytosis[60]) was performed by incubating cells at 37 °C with a 0.45 M sucrose solution; potassium (K^+) depletion (inhibiting clathrin-mediated endocytosis[61]), was performed by washing the cells (all at 37 °C) with PBS twice, followed by 5 min with hypotonic PBS (1:3 v/v with water), and five quick washes followed by 10 min incubation in K^+-depletion solution (150 mM NaCl, 1 mM $MgCl_2$, 1 mM $CaCl_2$, 2 mM HEPES pH 7.4, 0.5% DMSO, 0.5% BSA). Cellular ATP depletion was performed as in ref. 42 by washing cells twice followed by incubation for 30 min at 37 °C in 10 mM

2-deoxy-D-glucose, 10 mM NaN_3, 1 mM $MgCl_2$, 1 mM $CaCl_2$ in PBS. Control sample was prepared in 5 mM glucose, 1 mM $MgCl_2$, 1 mM $CaCl_2$ in PBS.

The following agonists, antagonists and growth factors were used: denopamine (β_1-AR selective agonist, Sigma D7815), isoproterenol (non-selective β-AR agonist, Sigma I5627), noradrenaline (β_1-AR agonist, Sigma, A7257), dobutamine (β_1-AR partial agonist, Sigma, D0676), terbutaline (β_2-AR selective agonist, Sigma, T2528), atenolol (β_1-AR selective antagonist, Sigma A7655), betaxolol (β_1-AR selective antagonist, Sigma B5683), butoxamine (β_2-AR selective antagonist, Sigma B1385), clonidine (α_2-AR selective agonist, Sigma C7897), dexmedetomidine (α_2-AR selective agonist, Tocris 2749), dopamine (dopamine receptor agonist, Sigma H8502), quinpirole (dopamine receptor 2 agonist, Sigma Q102), (+)-PD128907 (dopamine receptor 3 selective agonist, Tocris 1243), PD168077 (dopamine receptor 4 selective agonist, Tocris 1065), acetylcholine (muscarinic acetylcholine receptor agonist, Sigma A6625), VU152100 (muscarinic acetylcholine receptor 4 selective agonist, Tocris 3383), epidermal growth factor (EGF, Sigma E9644), Alexa Fluor 555-EGF (Life Technologies E35350), hepatocyte growth factor (HGF, Calbiochem 375228), fibroblast growth factor (FGF, Calbiochem 341591), vascular endothelial growth factor (VEGF, Calbiochem 676473), platelet-derived growth factor (PDGF, Calbiochem 521215), insulin-like growth factor 1 (IGF-1, Calbiochem 407251), transforming growth factor beta 1 (TGF-β1, Sigma T5050), bone morphogenetic protein 2 (BMP2, Cell Signaling Technologies 4697), nerve growth factor (NGF 2.5S, Invitrogen 13257-019), holo-transferrin (Sigma T0665), Alexa Fluor 488-Transferrin (Life Technologies T13342), Alexa Fluor 546-Transferrin (Life Technologies T23364), Alexa Fluor 633-Transferrin (Life Technologies T23362) and DiL-low density lipoprotein (DiI-LDL, Life Technologies L3482). Growth factors were labelled with Alexa-555 using a protein labelling kit (Life Technologies A37571), according to the instructions from the manufacturer.

Cell stimulation and cargo uptake. Cells were never serum-starved before stimulation and the ligand and antibodies were never pre-incubated with the cells at 4 °C. 'Resting' conditions correspond to cells being cultured in 10% serum media and directly fixed. '+ Serum' stimulation corresponds to the addition of 10% serum to regular culture media (final 20% serum concentration). Specific stimulations were performed as follow. HA–EGFP double tagged GPCRs: cells expressing HA–EGFP double-tagged GPCRs were stimulated at 37 °C, 5% CO_2 for 10 min in the presence of 10 μg ml^{-1} of anti-HA clone 16B12 monoclonal antibody and 10 μM of the ligands denopamine (HA–β_1AR–EGFP), isoproterenol (HA–β_2AR–EGFP), clonidine (HA–α_{2a}AR–EGFP and HA–α_{2b}AR–EGFP), dopamine (HA–DR1–EGFP and HA–DR5–EGFP), quinpirole (HA–DR2–EGFP), (+)-PD128907 (HA–DR3–EGFP), PD168077 (HA–DR4–EGFP), acetylcholine (HA–muR1–EGFP and HA–muR2–EGFP) or VU152100 (HA–muR4–EGFP). For microscopy experiments, cells expressing HA–β_1-AR–EGFP were incubated at 37 °C, 5% CO_2 for 4 min with 10 μg ml^{-1} anti-HA clone 16B12 monoclonal antibody and 10 μM denopamine. Adrenergic agonists and antagonists: cells were incubated at 37 °C for 4 min with 10 μM or a titrating range (10^{-8} to 10^{-5} M) of concentration of denopamine, isoproterenol, noradrenaline, dobutamine or terbutaline. In some experiments, cells were incubated with 10 μM atenolol, betaxolol, butoxamine 37 °C for 5 min before stimulation with isoproterenol. Growth factors: cells were incubated at 37 °C for 4 min with pre-warmed serum-free media containing 10 ng ml^{-1} of EGF, HGF, FGF, VEGF, PDGF, IGF-1 or NGF or 50 ng ml^{-1} BMP2 or 5 ng ml^{-1} TGF-β1 or 50 ng ml^{-1} Alexa Fluor 555-conjugated EGF, HGF, FGF, VEGF or IGF-1. In some experiments, EGF was titrated from 2 to 500 ng ml^{-1}. Anti-EGFR antibody feeding assays were performed by directly incubating cells with pre-warmed serum-free media containing 0.5 μg ml^{-1} of anti-EGFR clone 13A9 monoclonal antibody and 50 ng ml^{-1} of the indicated growth factors or 10 μM denopamine for 4 min at 37 °C. Interleukin-2: human T cells Kit255 were incubated at 37 °C with pre-warmed serum-free media containing either 200 pM IL-2 or 10 μg ml^{-1} anti-IL-2R clone 561 antibody and 200 pM IL-2 for the indicated time. Clathrin-independent cargoes: cells were incubated at 37 °C for 15 min with pre-warmed serum-free media containing 10 μg ml^{-1} of the indicated anti-CD proteins or MHC-I antibodies detecting the extracellular portion of the receptors. Clathrin-dependent cargoes: cells were incubated at 37 °C for 7 min with pre-warmed serum-free media containing 20 μg ml^{-1} Alexa Fluor-488-labelled human transferrin or 50 μg ml^{-1} DiL-LDL or for 15 min with media containing 10 μg ml^{-1} anti-TfR and anti-LDLR antibodies.

Sample processing and analysis. *Samples for microscopy.* After the incubation period at 37 °C, cells stimulated as described above were quickly washed once with 37 °C pre-warmed PBS to removed unbound ligands and antibodies and fixed with pre-warmed PFA 3.7% for 20 min at 37 °C. Fixed cells were then washed three washes three times with PBS and one time with PBS supplemented with 50 mM NH_4Cl to quench free PFA. Cells were then permeabilized (0.05% saponin), immunostained and imaged as described below.

Samples to be analysed by plate reader. After the incubation period at 37 °C, cells stimulated as described above were placed on ice to stop membrane traffic, washed with ice-cold PBS to removed unbound antibodies and incubated with Alexa-488-conjugated secondary antibodies on ice to label non internalized antibodies bound to receptors remaining on the cell surface. Cells were then washed twice with PBS, and fixed on ice with 3.7% PFA for 30 min. Cells were washed twice with PBS and once with 50 mM NH_4Cl in PBS and incubated with DAPI to label their DNA (used to normalized the number of cells in between samples and experiments). Signals from remaining (non-internalized) receptors and DAPI were measured using a FLUOstar Optima (BMG) plate reader.

Samples to be analysed by flow cytometry. After the incubation period at 37 °C, cells stimulated as described above were then placed on ice to arrest membrane traffic, washed with ice-cold PBS to removed unbound ligands, detached by 1 min incubation with 0.25% Trypsin-EDTA at 37 °C, spun, acid-washed (ice-cold stripping buffer (150 mM NaCl, 5 mM KCl, 1 mM $CaCl_2$, 1 mM $MgCl_2$, glycine) pH 2.5, three washes to remove surface-bound ligands), washed with PBS twice (to restore pH 7.4), fixed (PFA 3.7% for 20 min), washed and re-suspended in PBS and analysed using LSR II flow cytometer (Beckson-Dickinson).

Cell surface labelling. Cell surface staining of HA–GPCR–EGFP and EGFR was performed by incubating cells at 4 °C for 1 h with 10 μg ml^{-1} of anti-HA clone 16B12 monoclonal antibody or 10 μg ml^{-1} anti-EGFR 13A9 monoclonal antibody respectively, diluted in PBS containing 5% horse serum, followed by a quick wash with cold PBS and fixation (PFA 3.7% for 30 min at 4 °C followed by three washes with PBS and one wash with PBS supplemented with 50 mM NH_4Cl). Cells were then incubated with secondary antibodies diluted in 5% horse serum, and the coverslips were mounted with DABCO anti-fade agent on glass slides and imaged using the laser scanning confocal microscope described below. Signals were imaged by confocal microscopy or surface levels were measured using a FLUOstar Optima (BMG) plate reader.

Immunostaining, laser scanning confocal fluorescent microscopy and analysis. For ligand-induced endophilin-positive assemblies (EPAs), budding cells pre-incubated or not with inhibitors for 5 min were incubated at 37 °C for 4 min with pre-warmed imaging buffer containing the indicated ligands (note that no serum starvation or pre-incubations at 4 °C were performed), quickly rinsed with pre-warmed PBS and fixed (PFA 3.7% for 20 min at 37 °C followed with three washes with PBS and one wash with PBS supplemented with 50 mM NH_4Cl). Cells were then permeabilized (0.05% saponin) and immunostained (primary and secondary antibodies were diluted in 5% horse serum). In some experiments, DRAQ5 (DNA-binding dye, Cell Signaling Technologies 4084), phalloidin-tetramethylrhodamine (Santa Cruz Biotechnology sc-362065) or phalloidin-AlexaFluor 647 (Cell Signaling Technologies 8940) were added with secondary antibodies. The coverslips were mounted with DABCO anti-fade agent on glass slides and imaged using a laser scanning confocal microscope (TCS Sp5 AOBS; Leica) equipped with a 63× objective. For Alexa488, the illumination was at 488 nm and emission collected between 498 and 548 nm; for Alexa555 the laser illumination was at 543 nm and emission collected between 555 and 620 nm; for Alexa647 and DRAQ5, the laser illumination was at 633 nm and emission collected between 660 and 746 nm. For each quantification, the number of EPAs within 400 μm^2 masks were counted on confocal planes placed at the middle of three representative cells (from independent experiments). The percentages of co-localization of markers on EPAs or endophilin spots located at the leading edge of cells were determined using Volocity 6.0. The levels of endophilin (endogenous and EGFP-tagged constructs) and lamellipodin at the leading edges of cells were measured, for each condition, on masks covering a total at least 100 μm long (~ 2 μm wide) of leading edge of three cells from independent experiments using Volocity 6.0.

Immunostaining and plate reader measurements. Resting or stimulated cells grown on glass bottom 96-well plates were placed on ice to stop membrane traffic, washed with PBS to removed unbound ligands and fixed with 3.7% PFA for 30 min. Cells were washed twice with PBS and once with 50 mM NH_4Cl in PBS and permeabilized and immunostained with primary and secondary antibodies together with DAPI to label DNA (used to normalize the number of cells in between samples and experiments). Signals were measured using a FLUOstar Optima (BMG) plate reader.

Phosphoinositides staining and measurements. Cells grown in glass-bottom 96-well plates were fixed for 1 h at 37 °C with 3.7% (w/v) PFA, 0.1% glutaraldehyde and 0.15 mg ml^{-1} saponin in 5 mM KCl, 137 mM NaCl, 4 mM $NaHCO_3$, 0.4 mM KH_2PO_4, 1.1 mM Na_2HPO_4, 2 mM $MgCl_2$, 5 mM PIPES, pH 7.2, 2 mM EGTA and 5.5 mM glucose), as in ref. 62. Samples were then incubated for 90 min with primary antibodies diluted in 1% BSA, washed, stained with secondary antibodies together with DAPI to label DNA (used to normalize the number of cells in between samples and experiments). Signals were measured using a FLUOstar Optima (BMG) plate reader. The specificity of the antibodies was verified on cells overexpressing the PtdIns(4,5)P_2, PtdIns(3,4)P_2 and PtdIns(3,4,5)P_3-specific PH domains of PLCγ, TAPP1 and BTK, respectively.

Super-resolution microscopy. Cells were grown on 13 mm #1.5 Hecht Assistent coverslips and processed for immunofluorescence as described above with a few

modifications: for structured illumination microscopy (SIM) we used twice the amount of primary antibodies while for stimulated emission depletion microscopy (STED) both primary and secondary antibodies were used at five times its recommended concentration. Samples were and mounted using ProLong gold (Life Technologies). SIM images were acquired in Zeiss Elyra S.1 and processed using the Zeiss acquisition software ZEN. STED images were acquired in a Leica TCS SP8 X gated STED microscope equipped with a 592 depletion laser.

Immuno-electron microscopy. Control and stimulated (10 μM denopamine, 4 min at 37 °C) BSC1 cells grown on MatTek glass-bottomed Petri dishes were fixed in either 4% paraformaldehyde alone or with the addition of 0.05% glutaraldehyde in 0.1 M phosphate buffer, pH 7.4 overnight at 4 °C. After several buffer washes reactive aldehyde groups were inactivated using 0.1% sodium borohydride in phosphate buffer for 30 min, followed by permeabilization with 0.03% saponin in 20 mM phosphate buffer, 150 mM sodium chloride. Cells were then incubated in normal goat serum (Aurion) for 40 min before incubation with 0.5 μg ml^{-1} antibody against endophilin for 4.5 h at room temperature. After thorough washing, cells were incubated in a 1:200 dilution of goat anti rabbit ultrasmall gold (Aurion) overnight at 4°C. Cells were then fixed in 2% glutaraldehyde in phosphate buffer, washed with distilled water followed by silver enhancement of gold using R-Gent SE-EM (Aurion) reagents and post fixed with 0.5% osmium tetroxide in 0.1 M phosphate buffer on ice for 15 min. Cells were dehydrated in an ascending ethanol series and embedded in CY212 resin. Ultrathin sections were stained with saturated aqueous Uranyl Acetate and Reynolds Lead Citrate and examined using an FEI Technai Spirit EM operated at 80 kV.

Live-cell confocal fluorescent microscopy and analysis. Just before live-cell imaging, the medium of cells grown on MatTek dishes was changed to α-MEM without phenol red, supplemented with 20 mM HEPES, pH 7.4 and 5% FBS and placed into a temperature controlled chamber on the microscope stage with 95% air: 5% CO_2 and 100% humidity. Live-cell imaging data were acquired using a fully motorized inverted microscope (Eclipse TE-2000, Nikon) equipped with a CSU-X1 spinning disk confocal head (UltraVIEW VoX, Perkin-Elmer, England) using a 60× lens (Plan Apochromat VC, 1.4 NA, Nikon) under control of Volocity 6.0 (Improvision, England). 14-bit digital images were obtained with a cooled EMCCD camera (9100-02, Hamamatsu, Japan). Four 50 mW solid-state lasers (405, 488, 561 and 647 nm; Crystal Laser and Melles Griots) coupled to individual acoustic-optical tunable filter (AOTF) were used as light source to excite EGFP, Alexa488, TagRFP-T, Alexa555 and 647, as appropriate. Rapid two-colour time-lapses were acquired at 500 ms to 2 s intervals, using a dual (525/50; 640/120, Chroma) emission filter respectively. The power of the lasers supported excitation times of 50 ms in each wavelength and the AOTFs allowed minimum delay (~1 ms) between two colours (for example, delay between green–red for each time point), which was an important factor to assess the co-localization between markers.

Automated unbiased identification of all AP2 fluorescent spots and quantitative tracking of their dynamics as a function of time were performed as in ref. 49. Endophilin-positive assembly (EPA) budding rates represent the number of new EPAs per 5×10^4 μm^2 per second, normalized to the average of the control captures. Co-localization scorings were performed on at least 100 EPAs at the plasma membrane, from three cells imaged during independent experiments.

Signal transduction and immunoblotting. Cells grown on 6-well plates were transfected with siRNAs and transferred to 24-well plates on the following day. Three days after transfection cells were serum starved for 4 h and stimulated at 37 °C with 5 or 100 ng ml^{-1} EGF diluted in serum-free α-MEM (Life Technologies) for the indicated times. After each time points, cells were quickly collected in Laemmli sample buffer, sonicated and boiled. Samples were run on NuPage 4–12% Bis-Tris gel (Life Technologies), transferred to nitrocellulose membranes, blocked in 5% skimmed milk and incubated successively with primary and secondary-HRP coupled antibodies and finally visualized with ECL Plus, Pico or Femto (Thermo) reagents depending on the strength of the signals. Signals were captured on a BioRad Geldoc XR+ system and analysed using the ImageLab software (BioRad). Signals used for quantifications were captured at a pre-saturation intensity. Signals were normalized to the time point zero or 30 of the control sample for the 5 ng ml^{-1} and 100 ng ml^{-1} experiments, respectively.

cAMP was measured using the Cyclic AMP XP chemiluminescent assay kit (Cell Signaling Technologies, 8019) following the manufacturer's instructions. Signals were measured on a FLUOstar Optima plate reader (BMG).

PathScan Intracellular Signalling and EGFR Signalling Antibody Arrays (Cell Signaling Technology 7744 and 12785, respectively) were used according to the manufacturer and fluorescent signals were measured using an Odyssey (LI-COR) reader.

Plasma membrane isolation. Cell surface protein isolation, excluding intracellular proteins, was performed by selective biotinylation using a cell-impermeable, cleavable biotinylation reagent (Sulfo-NHS-SS-Biotin) followed by purification of surface proteins by affinity-purified NeutrAvidin Agarose Resin (Thermo Scientific 89881).

Wound-healing cell migration assay. BSC1 and RPE1 cells were grown in 6-well plates in their respective media for 24 h. A mechanical wound was introduced in the middle of the confluent layers of cells and the cells were allowed to grow in fresh media supplemented or not with the indicated inhibitors at 37 °C. Images were taken immediately after the wound and regularly until the end of the assay (16 h). Cell migration was measured by the reduction of free space between the two pictures and normalized to the mean of control cells.

PC12 neurite outgrowth assay. PC12 cells were grown in in RPMI 1640 containing 7.5% heat-inactivated horse serum, 7.5% FBS and subcultured using trypsin in type IV collagen coated flasks (BD Biocoat, Cat No 354523). Cells were detached, re-suspended in PBS, counted and electroporated with 20 pmol siRNA in 10 μl tips using a Neon electroporation system (Life Technologies) set to a single pulse of 1,410 V for 30 ms. Cells were immediately transferred to warmed medium containing or not NGF (2.5S subunit, 100 ng ml^{-1}) and plated onto dishes coated with poly-L-lysine/type I collagen 25:1 at a density of 1×10^4 cells cm^{-2}. After 2 days, cells were re-transfected with silencing RNAs using Lipofectamine RNAi MAX according to manufacturer's instructions. Cells were re-fed with or without NGF every 48 h.

Statistical analysis. Results shown are mean ± standard error of the mean (s.e.m.). Statistical testing was performed using Prism 6 (GraphPad Software). Data were tested for Gaussian distribution with Kolmogorov–Smirnov test with the Dallal–Wilkinson–Lillie for corrected P value. In case of Gaussian distribution, the following parametric tests were used: Student's t-test (2 groups) or one-way ANOVA and Dunnett's test (2+ groups), as appropriated. In case of non-Gaussian distribution, the following non-parametric tests were used: two-tailed Mann–Whitney U-test (2 groups) or Kruskal–Wallis one-way ANOVA and Dunnett's test (2+ groups), as appropriated.

Significance of mean comparison is annotated as follow: NS, not significant; $*P < 0.05$; $**P < 0.01$; $***P < 0.001$. No statistical methods were used to predetermine sample size.

45. Shaner, N. C. *et al.* Improving the photostability of bright monomeric orange and red fluorescent proteins. *Nature Methods* **5,** 545–551 (2008).
46. Usami, Y., Popov, S. & Gottlinger, H. G. Potent rescue of human immunodeficiency virus type 1 late domain mutants by ALIX/AIP1 depends on its CHMP4 binding site. *J. Virol.* **81,** 6614–6622 (2007).
47. Ford, M. G. *et al.* Simultaneous binding of PtdIns(4,5)P_2 and clathrin by AP180 in the nucleation of clathrin lattices on membranes. *Science* **291,** 1051–1055 (2001).
48. Marks, B. *et al.* GTPase activity of dynamin and resulting conformation change are essential for endocytosis. *Nature* **410,** 231–235 (2001).
49. Henne, W. M. *et al.* FCHo proteins are nucleators of clathrin-mediated endocytosis. *Science* **328,** 1281–1284 (2010).
50. Motley, A., Bright, N. A., Seaman, M. N. & Robinson, M. S. Clathrin-mediated endocytosis in AP-2-depleted cells. *J. Cell Biol.* **162,** 909–918 (2003).
51. Subtil, A., Hemar, A. & Dautry-Varsat, A. Rapid endocytosis of interleukin 2 receptors when clathrin-coated pit endocytosis is inhibited. *J. Cell Sci.* **107,** 3461–3468 (1994).
52. Pelish, H. E. *et al.* Secramine inhibits Cdc42-dependent functions in cells and Cdc42 activation in vitro. *Nature Chem. Biol.* **2,** 39–46 (2006).
53. Macia, E. *et al.* Dynasore, a cell-permeable inhibitor of dynamin. *Dev. Cell* **10,** 839–850 (2006).
54. Howes, M. T. *et al.* Clathrin-independent carriers form a high capacity endocytic sorting system at the leading edge of migrating cells. *J. Cell Biol.* **190,** 675–691 (2010).
55. Hill, T. A. *et al.* Inhibition of dynamin mediated endocytosis by the dynoles–synthesis and functional activity of a family of indoles. *J. Med. Chem.* **52,** 3762–3773 (2009).
56. Joshi, S. *et al.* The dynamin inhibitors MiTMAB and OcTMAB induce cytokinesis failure and inhibit cell proliferation in human cancer cells. *Mol. Cancer Ther.* **9,** 1995–2006 (2010).
57. Schlegel, R., Dickson, R. B., Willingham, M. C. & Pastan, I. H. Amantadine and dansylcadaverine inhibit vesicular stomatitis virus uptake and receptor-mediated endocytosis of alpha 2-macroglobulin. *Proc. Natl Acad. Sci. USA* **79,** 2291–2295 (1982).
58. Wang, L. H., Rothberg, K. G. & Anderson, R. G. Mis-assembly of clathrin lattices on endosomes reveals a regulatory switch for coated pit formation. *J. Cell Biol.* **123,** 1107–1117 (1993).
59. Gibson, A. E., Noel, R. J., Herlihy, J. T. & Ward, W. F. Phenylarsine oxide inhibition of endocytosis: effects on asialofetuin internalization. *Am. J. Physiol.* **257,** C182–C184 (1989).
60. Heuser, J. E. & Anderson, R. G. Hypertonic media inhibit receptor-mediated endocytosis by blocking clathrin-coated pit formation. *J. Cell Biol.* **108,** 389–400 (1989).
61. Larkin, J. M., Brown, M. S., Goldstein, J. L. & Anderson, R. G. Depletion of intracellular potassium arrests coated pit formation and receptor-mediated endocytosis in fibroblasts. *Cell* **33,** 273–285 (1983).
62. Yip, S. C. *et al.* Quantification of PtdIns(3,4,5)P_3 dynamics in EGF-stimulated carcinoma cells: a comparison of PH-domain-mediated methods with immunological methods. *Biochem. J.* **411,** 441–448 (2008).

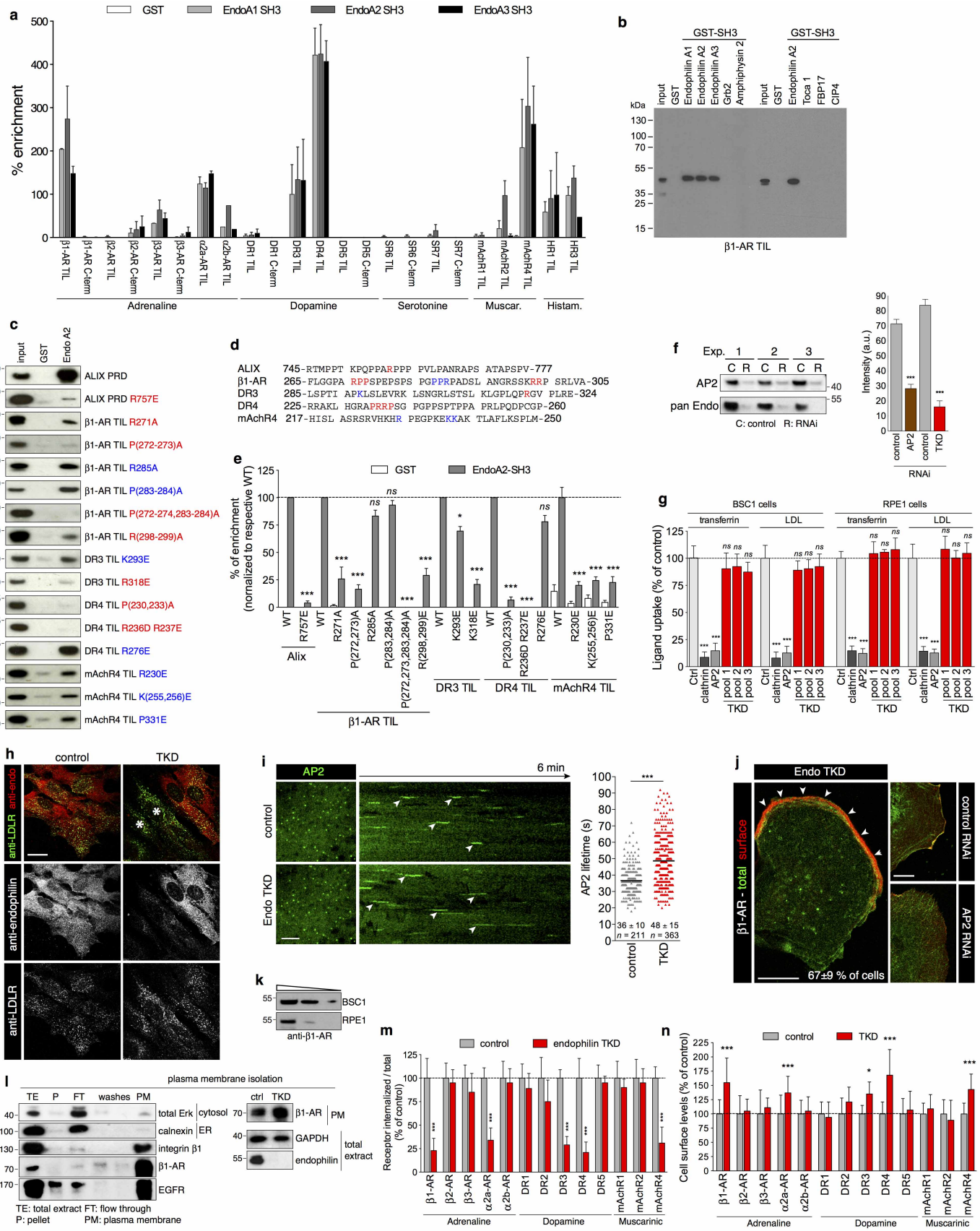

Extended Data Figure 1 | Endophilin binds to some GPCRs and is dispensable for clathrin-mediated endocytosis. Related to Fig. 1. **a**, Quantification of the binding of indicated cytosolic fragments of adrenergic, dopaminergic, serotoninergic, muscarinic (Muscar.) and histaminergic (Histam.) receptors (see Fig. 1a for an example of one set of immunoblots) to the indicated GST–SH3 domains (or GST as control). The percentage enrichment of receptor tails in pulled-down fractions with respect to their respective levels in the original cell extracts (input) is shown (mean ± s.e.m., $n = 3$ independent experiments). **b**, Binding of GST–SH3 domains from BAR and F-BAR containing proteins to β_1-AR third intracellular loop (TIL), showing specificity for endophilin-A SH3 domains. **c**, Pull-down experiments using GST–SH3 domains of endophilin-A2 (or GST as a control) with EGFP-tagged fragments coding for the TILs of the indicated receptors bearing the depicted mutations. Mutations decreasing binding are shown in red; the ones without significant effects are in blue. ALIX PRD domain and its R757E mutant[58] were used as positive and negative controls. **d**, Amino acid sequence around point mutations tested showing potential endophilin-binding motifs. **e**, Quantification of the binding of indicated mutated cytosolic fragments (see **c** for an example of one set of immunoblots) to the indicated GST–SH3 domains (or GST as control). The percentage enrichment of receptors tails in pulled-down fractions with respect to their respective levels in the original cell extracts (input) is shown (means ± s.e.m. from three independent experiments; NS, non-significant, $*P < 0.05$, $***P < 0.001$, one-way ANOVA and Dunnett's test versus respective wild-type). **f**, Verification of AP2 and Endo1+2+3 depletion by RNAi from three independent control ('C') and RNAi ('R') experiments. Immunoblot (left) and bar graph (right) representations of the data are shown (means ± s.e.m. from three independent experiments; $***P < 0.001$, Student's *t*-test versus respective control). **g**, Transferrin and LDL uptake was inhibited by clathrin and *AP2* RNAi but not by control (Ctrl) or endophilin-A triple RNAi (TKD, three different pools). Ligand uptake was measured by flow cytometry (mean ± s.e.m., 10,000 cells per experiment, $n = 3$ independent experiments; NS, non-significant, $***P < 0.001$, one-way ANOVA and Dunnett's test versus respective control). **h**, Anti-LDLR antibody uptake assay in control or TKD RPE1 cells. Cells were immunostained for anti-LDLR (post feeding) and endophilin (red). Cells strongly depleted for endophilin (*) showed similar LDLR endocytosis to control cells, showing that LDLR endocytosis is not dependent on endophilin-A proteins (images representative of ten captures). **i**, Dynamics of clathrin-coated pits in BSC1 cells marked by σ2-EGFP (AP2) and acquired by live-cell spinning-disk confocal microscopy imaging. Left pictures show representative images from the bottom surface of cells; right pictures are kymographs (time projections) representative of five captures from control and Endo1+2+3 RNAi cells. Right: plot of individual lifetimes of clathrin/AP2 pits calculated from live imaging of 4 cells for each condition. Those had significant longer lifetimes in TKD cells, perhaps related to a reduced synaptojanin recruitment to membranes and thus an increase in PtdIns(4,5)P_2 levels[5,20] (bars, means; $n = 211$ and 363 from 3 independent experiments, mean ± s.e.m. is written at the bottom, $***P < 0.001$, Mann–Whitney *U*-test). **j**, Surface staining of β_1-AR using the HA–β_1-AR–EGFP construct. Control, *AP2* RNAi and endophilin TKD cells were directly stained for steady-state accumulation of β_1-AR at their cell surface and imaged using a confocal microscope (images are representative of five captures). In endophilin TKD cells β_1-AR accumulated in a limited area of the plasma membrane, similar to the area stained with lamellipodin in Extended Data Fig. 2c. This panel complements that in Fig. 1b showing a lack of internalization of β_1-AR in TKD cells. **k**, Immunoblots showing the expression of β1 adrenergic receptor (β_1-AR) in BSC1 and RPE1 cells. Decreasing amount of cell extracts were loaded from left to right. **l**, Left: isolation of a plasma membrane fraction (see Methods) showed accumulation of β1-adrenergic receptors after endophilin RNAi. Erk was used to monitor cytosolic proteins, calnexin endoplasmic reticulum proteins and integrin β1, β1-adrenergic receptor (β_1-AR) and EGFR to monitor plasma membrane proteins. Note that the plasma membrane fraction (PM) was enriched in plasma membrane proteins and did not contain cytosolic ERK or ER-localized calnexin. Right: levels of β_1-AR were enriched in the plasma membrane fraction from TKD cells versus control cells. **m**, Bar graph shows the amounts of internalized/total depicted HA–receptor–EGFP in control (grey) or endophilin TKD (red) samples (mean ± s.e.m., $n = 3$ independent experiments; $***P < 0.001$, Student's *t*-test versus respective control). **n**, Surface staining of HA–receptor–EGFP constructs (see Fig. 1b, c). Cells were directly stained with anti-HA antibody at 4 °C and measured using a plate reader to assay the steady-state accumulation of receptors at the cell surface. The cell surface signals (HA) were corrected for expression levels (EGFP) and the values were normalized to the mean of the control cells (mean ± s.e.m., $n = 3$ independent experiments; $***P < 0.001$, Student's *t*-test versus respective control). The same receptors that showed a decreased endocytosis (**m**) show an increased surface accumulation here, an effect that is dependent on ligand activation. Scale bars: 20 μm (**h**), 10 μm (**j**) and 5 μm (**i**).

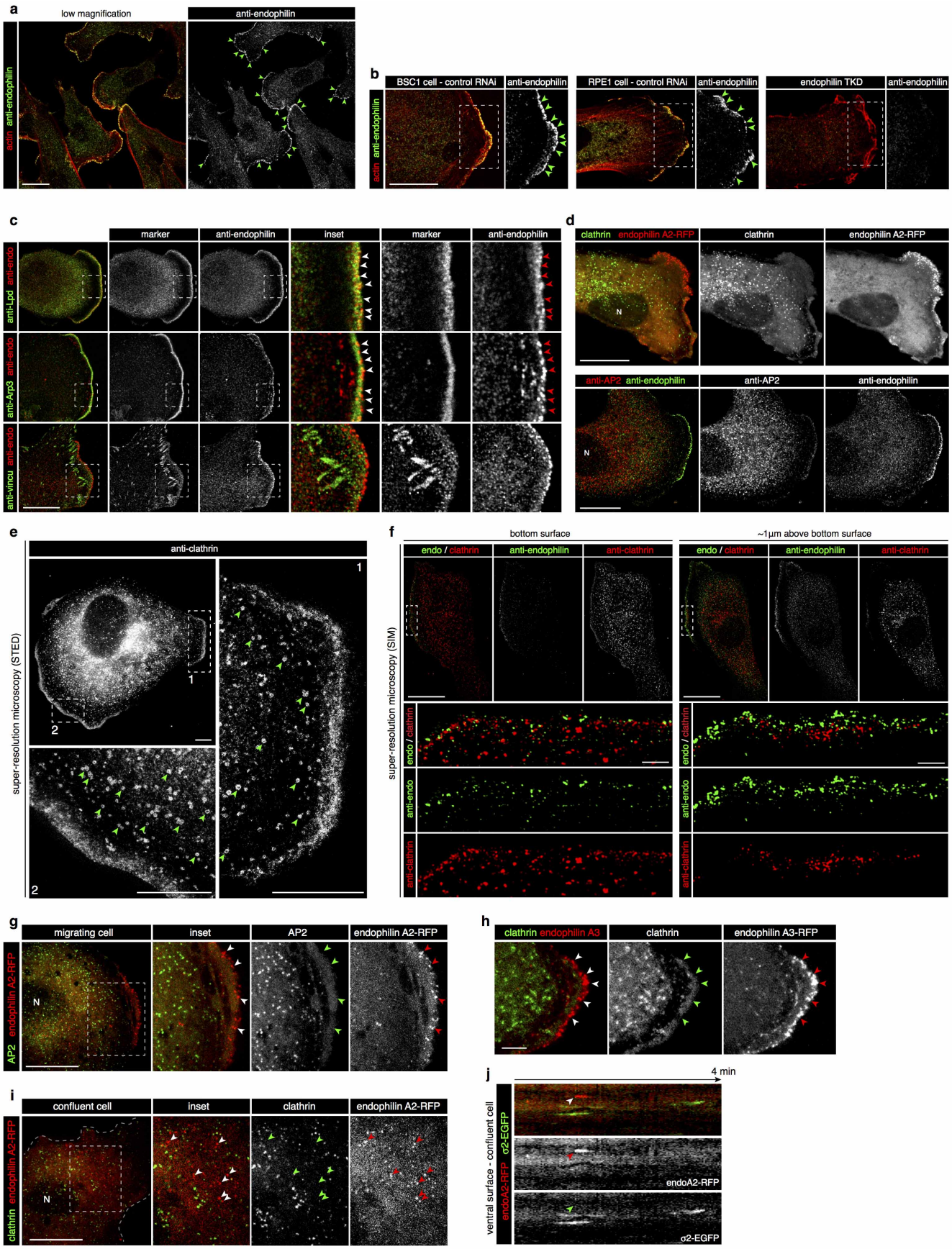

Extended Data Figure 2 | Endophilin and clathrin did not co-localize at the leading edge of cells by standard and super-resolution microscopy. Related to Fig. 1. **a**, **b**, Confocal microscopy images (optical planes from the middle of cells) showing endogenous staining of endophilin (green) in BSC1 cells (low magnification in **a** and higher magnification in **b**, left panel) and in a normal diploid RPE1 cell (middle). Images in **b** were oriented with leading edges (identified by phalloidin staining (actin, red)) pointing to the right. Arrowheads point to endophilin puncta on the leading edge of these cells. Right: there was no anti-endophilin staining in endophilin-A TKD cells, validating the specificity of the antibody. Insets are zooms of the boxed areas. **c**, Confocal microscopy images showing endogenous staining of lamellipodin, Arp3 or vinculin (all green) and endophilin (red) in BSC1 cells. Insets are zooms of the boxed areas. Endophilin co-localized with lamellipodin and Arp3 at the leading edge but not with vinculin (a marker of focal adhesions). **d**, Top: same data as in Fig. 1c but showing the individual channels. Confocal microscopy images showing clathrin (EGFP–LCa, green) and endophilin (endophilin A2–RFP, red) in a live BSC1 cell. 'N' denotes the nucleus. Bottom: confocal microscopy images showing endogenous staining of α-adaptin (AP2), and endophilin (red) in BSC1. Endogenous staining also shows an enrichment of endophilin at the leading edge. **e**, Super-resolution stimulated emission depletion (STED) microscopy images of a BSC1 cell immunostained for clathrin and showing coated pits and vesicles labelled at the ventral surface of the cell but not at the leading edges where the staining was diffused. **f**, Super-resolution structured illumination microscopy (SIM) images of a BSC1 cell immunostained for clathrin (red) and endophilin (green). Note the absence of co-localization between the two markers. **g**, Confocal microscopy images (bottom surface optical section) showing the localization of AP2 (σ2-EGFP, green) and endophilin (EndoA2–RFP, red) in a live migrating cell. Arrowheads point to endophilin A2 puncta at the leading edge of the cell; these are negative for AP2. Inset is a zoom of the boxed area. **h**, Confocal microscopy images showing a lack of co-localization of clathrin (EGFP–LCa, green) and the other endophilin-A expressed in BSC1 cells: endophilin A3 (endophilin A3–RFP, red). Arrowheads point to endophilin A3 puncta at the leading edge of live BSC1 cells; these are negative for clathrin puncta. **i**, Confocal microscopy images (optical section of bottom surface) showing clathrin (EGFP–LCa, green) and endophilin (EndoA2–RFP, red) localization in a live confluent BSC1 cell (thus no leading edge). Neighbouring cells were not transfected. Arrowheads point to endophilin A2 puncta at the bottom surface of the cell; most of these are negative for AP2. Inset is a zoom of the boxed area. **j**, Representative kymographs of AP2 (σ2–EGFP) and endophilin (EndoA2–RFP) from live-cell imaging acquired at the ventral surface of a confluent cell. The arrowhead points to an endophilin-positive track devoid of AP2. Images and kymographs are representative of at least ten captures, from three independent experiments. Scale bars: 20 μm (**a**, **d**), 10 μm (**b**, **c**, **f**, **e**), 5 μm (**e**, **h**) and 1 μm (**f** insets).

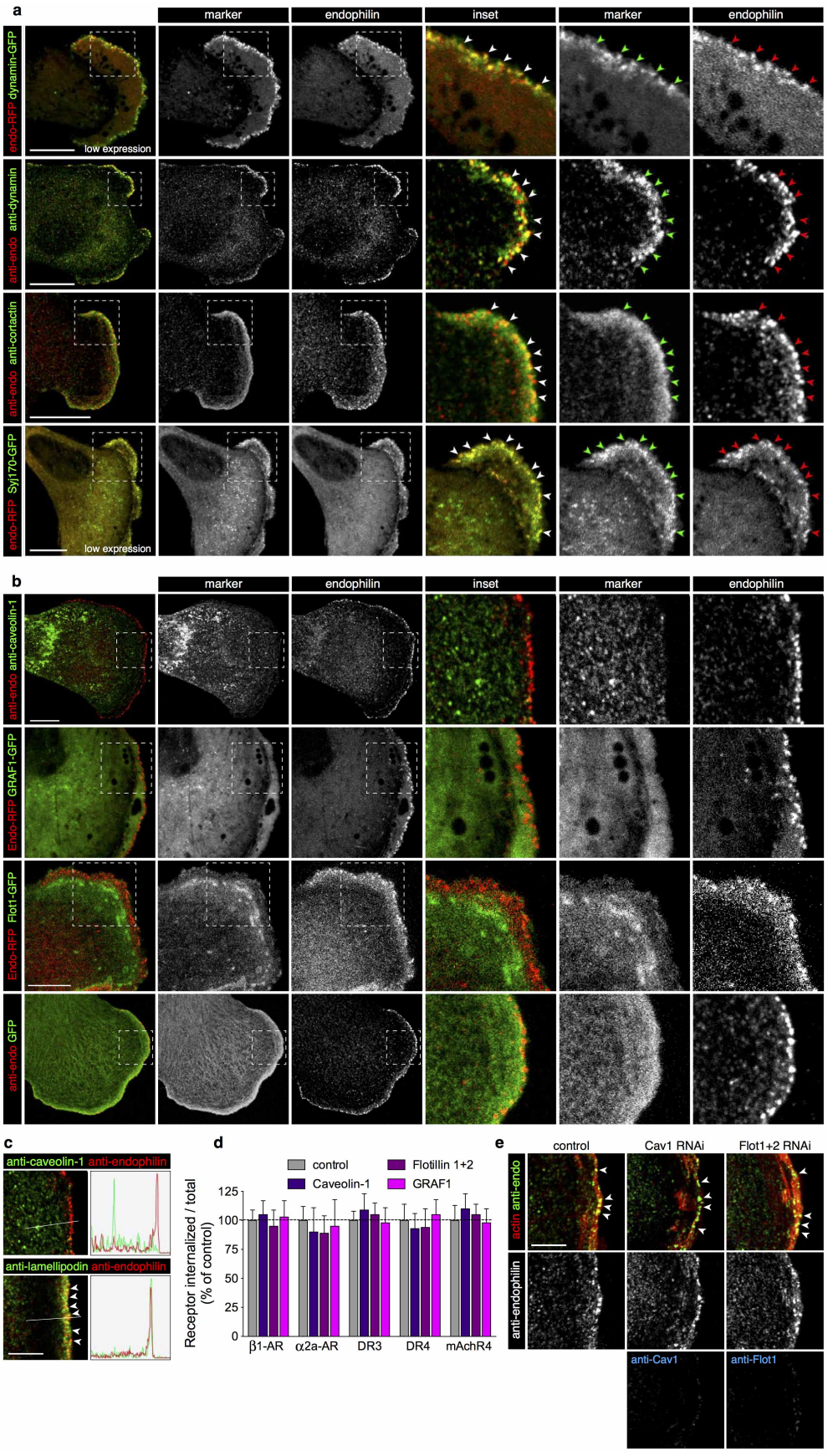

Extended Data Figure 3 | Endophilin co-localized with dynamin, cortactin and synaptojanin but not with known clathrin-independent endocytosis markers. Related to Fig. 1. **a**, Representative confocal images showing the co-localization of endophilin (endoA2–RFP or anti-endophilin, red) with dynamin (dynamin2–EGFP expressed at low levels, or anti-dynamin for endogenous protein (green)), cortactin (anti-cortactin for endogenous protein) or synaptojanin (synaptojanin 1-170–EGFP expressed at low levels). Insets are zooms of the boxed areas. **b**, Representative confocal images showing the absence of co-localization between endophilin (anti-endophilin, or endoA2–RFP, red) and caveolin 1 (endogenous), GRAF1–EGFP and flotillin 1–EGFP. The bottom row shows the background co-localization of endophilin with a soluble protein (EGFP). Arrowheads point to endophilin puncta at the leading edge of cells; these were negative for the markers tested. Insets are magnifications of the boxed areas. **c**, Co-localization of endogenous endophilin (red) with lamellipodin, but not caveolin-1 (green). Images were oriented with the leading edges to the right. Arrowheads point to co-localization between markers. Intensity profiles were acquired along the indicated lines. **d**, Receptor uptake assay (HA–receptor–EGFP internalized corrected for their total levels) in cells pre-treated with the indicated RNAi (mean ± s.e.m., $n = 3$ independent experiments). **e**, Confocal images of cells treated with caveolin-1 (Cav1) or flotillin 1 and 2 (Flot1+2) or control siRNA and immunostained for endophilin (green) and actin (red). Cells were counter-stained (blue) for caveolin 1 (Cav1) or flotillin-1 (Flot1) to ascertain for the depletion of the targeted proteins in the cells imaged. Images are representative of at least ten captures, from three independent experiments. Scale bars: 10 μm (**a**) and 5 μm (**b**, **c** and **e**).

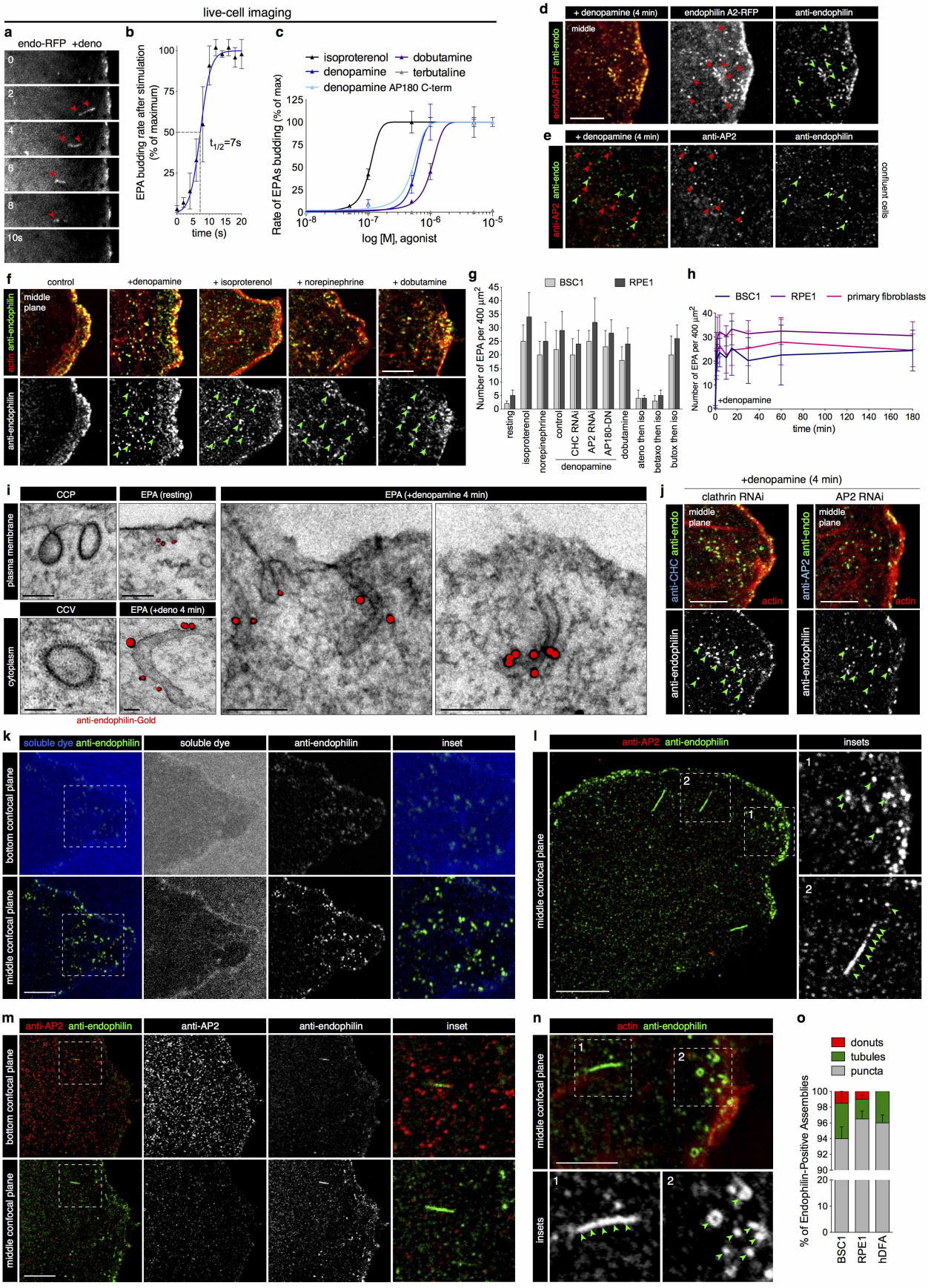

Extended Data Figure 4 | Formation of endophilin-positive tubules and vesicles upon β1-adrenergic receptor activation. Related to Fig. 1. **a**, Images from a time-lapse acquired by spinning-disk confocal microscopy of a BSC1 cell expressing low levels of endophilin-A2–RFP, after addition of 10 μM of denopamine ($t = 0$). Arrowheads point to a tubulo-vesicular carrier formed upon stimulation and moving from the cell edge (right) to the cell centre (left). See also Supplementary Video 3. **b**, The budding rate of endophilin-positive assemblies (EPAs), measured as number of EPAs $\mu m^{-2} s^{-1}$, after stimulation with denopamine (added at $t = 0$). Data were acquired from data sets similar to Supplementary Video 3 and normalized to the maximum budding rate (mean ± s.e.m., $n = 3$ independent experiments). **c**, Budding of endophilin–mRFP-positive structures determined by live-cell imaging after addition of various β_1-AR (isoproterenol, dobutamine and denopamine) or β_2-AR (isoproterenol, terbutaline) agonists concentrations. Data are expressed as the percentage of maximum budding. See also Supplementary Video 3. Terbutaline, the specific β_2-AR agonist, does not stimulate EPA production. Inhibition of clathrin-mediated endocytosis by AP180 C terminus expression does not affect EPA formation stimulated by the β_1-AR agonist denopamine (mean ± s.e.m., $n = 3$ independent experiments). **d**, Representative confocal images (optical planes located at the middle of cells) showing the co-localization of endophilin A2–RFP (red) with endogenous endophilin (green) in a BSC1 cell stimulated with denopamine (10 μM for 4 min), validating the targeting of exogenously expressed endophilin in our experiments. **e**, Representative confocal images (optical section located at the middle of cells) of confluent cells stimulated for 4 min with 10 μM denopamine and stained for endogenous endophilin (green) and α-adaptin (AP2, red). **f**, Representative confocal images (optical section located at the middle of cells) of sparse (**f**) or confluent (**e**) cells stimulated for 4 min with the indicated adrenergic agonists and stained for endogenous endophilin (green) and actin (phalloidin, red). **g**, Quantification of EPAs in BSC1 and RPE1 cells upon stimulation with adrenergic receptor agonists in control, *AP2* RNAi or AP180 dominant-negative-expressing cells or in cells pre-treated (5 min) with beta-blockers before stimulation (mean ± s.e.m., $n = 3$ independent experiments). **h**, Quantification of the number of endogenous EPAs per 400 μm^2 in BSC1, RPE1 cells and in primary fibroblasts upon stimulation with 10 μM denopamine for the indicated amounts of time (mean ± s.e.m., $n = 3$ independent experiments). **i**, Immuno-electron microscopy of BSC1 cells fixed 4 min after addition of 10 μM denopamine (deno) to the medium or in absence of stimulation (control). Anti-endophilin antibodies were detected with a gold-conjugated secondary antibody (red balls). The two pictures on the left show clathrin-coated pits (top) and a potential vesicle (bottom). The other images are membrane structures at the plasma membrane and in the cytoplasm positive for the anti-endophilin antibody (endogenous endophilin). **j**, Representative confocal images (optical section located at the middle of cells) of cells depleted for clathrin (left, same image as in Fig. 1e) or AP2 and stimulated with denopamine (10 μM) for 4 min before fixation. Endogenous endophilin (green) clathrin or AP2 (blue) and actin (phalloidin, red) were immunostained. **k**, Confocal microscopy images of a stimulated (10 μM denopamine for 4 min) RPE1 cell grown on a poly-lysine-coated coverslip, incubated in soluble lysine-fixable Alexa647 dye, fixed and immunostained for endophilin (green). On the confocal plane taken at the bottom of the cell (dye in focus), no endophilin spots can be seen (out of focus). On a confocal plane at the middle of the cell (dye outlines the cell cross-section) EPAs are in focus, indicating that they are in the cytoplasm and not at the cell surface. **l**, Example of a BSC1 cell treated and immunostained as in **m** and imaged at the middle of the cell and showing several endophilin-positive tubules and diffraction-limited puncta. **m**, Confocal microscopy images of a stimulated (10 μM denopamine for 4 min) BSC1 cell fixed and immunostained for α-adaptin (AP2, red) and endophilin (green). On the confocal plane taken at the bottom of the cell AP2 spots (known to be located at the plasma membrane) are in focus but EPAs are out of focus. On a confocal plane at the middle of the cell AP2 spots are out of focus but EPAs are in focus, indicating that they are inside the cytoplasm and not at the plasma membrane. **n**, Confocal microscopy images of EPAs labelled by endophilin. Arrowheads show diffraction-limited punctates, tubules and 'doughnut-like' vesicles structures. **o**, Quantification of the occurrence in stimulated BSC1, RPE1 and human primary dermal fibroblasts of the three different endophilin-positive structures: diffraction-limited punctates (grey), tubules (green) and 'doughnut-like' vesicles (mean ± s.e.m., $n = 3$ independent experiments). Images are representative of at least ten captures, from three independent experiments. Scale bars: 5 μm apart from **i**, which is 250 nm.

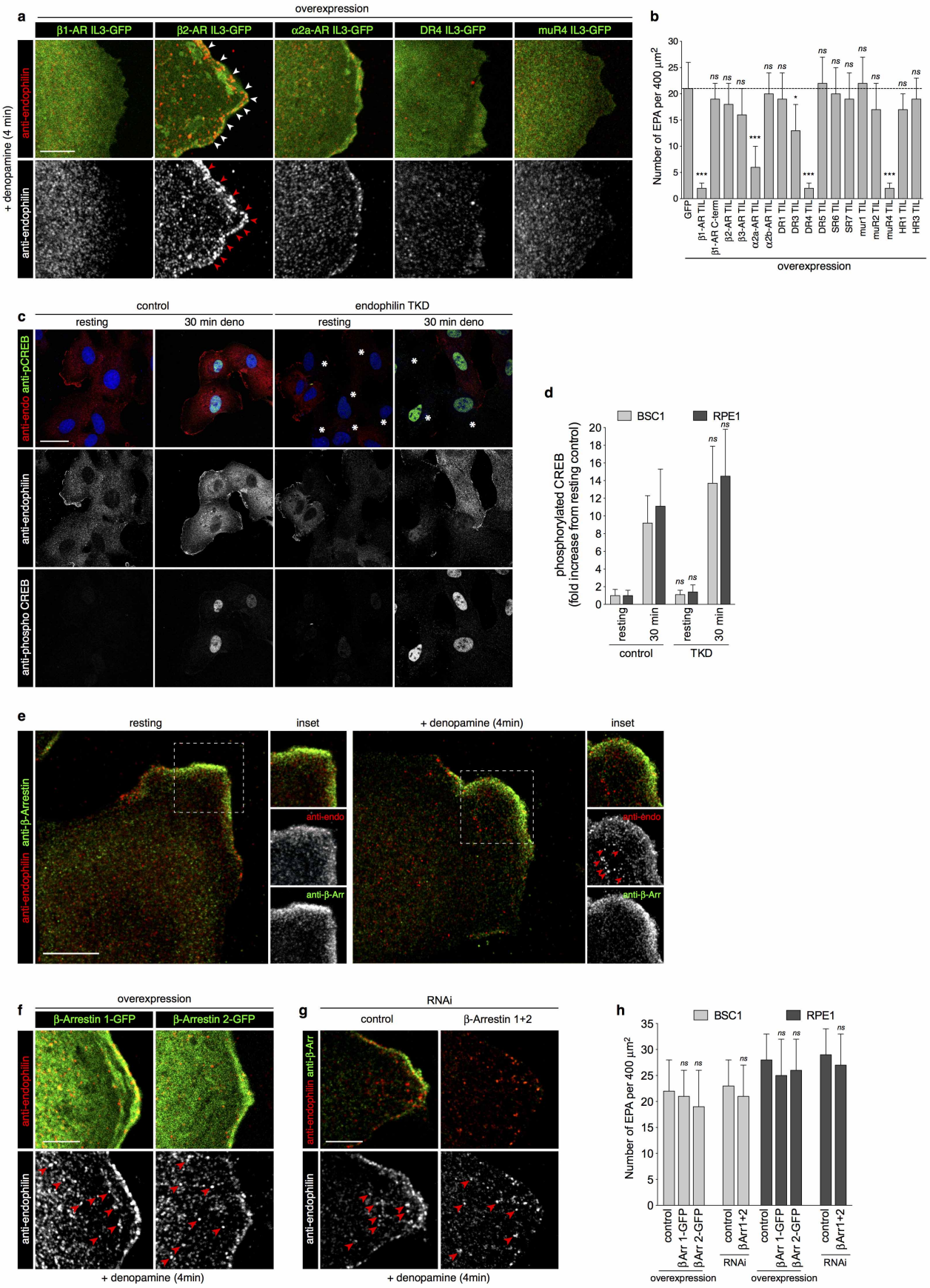

Extended Data Figure 5 | β1 and β2 arrestins were not essential in β1-adrenergic receptor agonist stimulation of endophilin vesicle formation. Related to Fig. 1. **a**, Representative confocal images (optical planes located at the middle of cells) of cells overexpressing the indicated EGFP-tagged receptors TIL (green), stimulated with 10 μM denopamine for 4 min and immunostained for endophilin (red) (images are representative of ten captures from three independent experiments). **b**, Quantification of the number of endogenous EPAs in cells overexpressing the indicated EGFP-tagged receptors TIL and stimulated with 10 μM denopamine for 4 min (mean ± s.e.m., $n = 3$ independent experiments; NS, non-significant, $^{*}P < 0.05$, $^{***}P < 0.001$, one-way ANOVA and Dunnett's test versus GFP). **c**, Confocal microscopy images of control and endophilin TKD cells, resting or stimulated (10 μM denopamine for 4 min) and immunostained for phosphorylated CREB (pCREB, green), endophilin (red) and DNA (DRAQ5, blue) (images are representative of ten captures from three independent experiments). Asterisks denote cells with strongly reduced endophilin levels. **d**, Plate reader quantification of BSC1 or RPE1 cells treated as in **a** (mean ± s.e.m., $n = 3$ independent experiments; NS, non-significant, Student's *t*-test versus respective control). **e**, Confocal microscopy images of control and stimulated (10 μM denopamine for 4 min) cells immunostained for β-arrestin (green) and endophilin (red). EPAs (arrowheads) did not contain β-arrestin (images representatives of ten captures from three independent experiments). **f**, **g**, Confocal microscopy images of cells overexpressing β-arrestin-1 or 2-EGFP (**f**, green) or β-arrestin 1+2 KD cells (**g**), stimulated with denopamine (10 μM for 4 min), fixed and immunostained for endophilin (red) and β-arrestin (**g**, green) (images representatives of at least ten captures). **h**, Plate reader quantification of BSC1 or RPE1 cells treated as in **e**–**g** (mean ± s.e.m., $n = 3$ independent experiments; NS, non-significant, one-way ANOVA and Dunnett's test versus respective controls). Scale bars: 40 μm (**c**) and 5 μm (**a**, **e**–**g**).

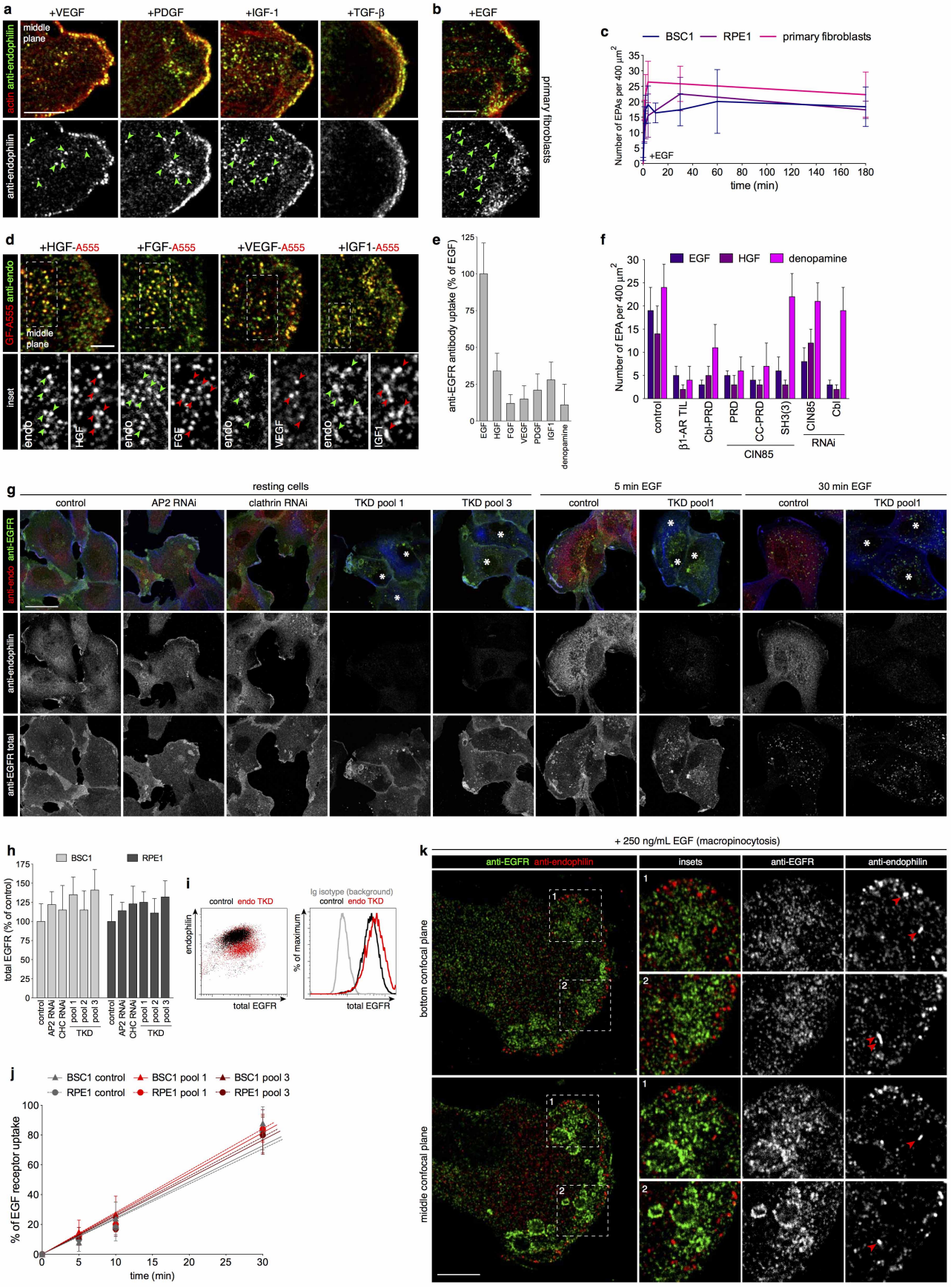

Extended Data Figure 6 | Several growth factors stimulated the formation of endophilin-positive assemblies. Related to Fig. 2. **a**, Confocal images (optical planes from the middle of cells) of BSC1 cells treated for 4 min with the indicated growth factors (all at 10 ng ml^{-1}) and immunostained for endogenous endophilin-A (green). Cells were oriented with their leading edges (identified with phalloidin staining (actin, red)) pointing to the right (images are representative of ten captures from three independent experiments). Arrowheads show internal vesicles positive for endogenous endophilin in the VEGF, PDGF and IGF-1-treated but not TGF-β-treated cells (see also quantification in Fig. 2c). **b**, EPA production in a primary fibroblast from an adult donor treated for 4 min with 50 ng ml^{-1} EGF and immunostained for endogenous endophilin-A (green). The image is representative of eight captures. **c**, Quantification of the number of endogenous EPAs per 400 μm^2 in BSC1, RPE1 cells or primary fibroblasts upon stimulation with 50 ng ml^{-1} EGF for the indicated amounts of time (mean ± s.e.m., $n = 3$ independent experiments). **d**, Confocal section of a BSC1 cell fixed 4 min after addition of 50 ng ml^{-1} Alexa555-labelled EGF, HGF, FGF, VEGF and IGF-1 to the medium. Endogenous endophilin (green) was detected as in **a**. Arrowheads point to internal vesicles positive for endogenous endophilin and containing internalized growth factors (images are representatives of at least eight captures). **e**, Plate reader quantification of BSC1 cell incubated with a monoclonal antibody anti-EGFR (13A9, green), that does not interfere with EGF binding, and 50 ng ml^{-1} of the indicated ligands. There is no cross-talk between EGFR and activation of other growth factor receptors or activation of β1 adrenergic receptors. Thus, endophilin-positive structures only have EGFR when stimulated by EGF (see Fig. 2d, e), and likewise on β1 adrenergic receptor activation there is no EGFR in the endophilin-positive structures. This reinforces the theme that one needs specific receptor activation to transduce a signal across the membrane to activate EPA formation (mean ± s.e.m., $n = 3$ independent experiments). **f**, Quantification of the number of EPAs in cells depleted for CIN85 or Cbl or overexpressing β_1-AR TIL, Cbl-PRD or CIN85-PRD, -CC-PRD, SH3(3) and stimulated with EGF (blue), HGF (purple) or denopamine (fuchsia) (mean ± s.e.m., $n = 3$ independent experiments). **g**, Confocal images of control, AP2, clathrin or endophilin TKD (pools 1 and 3) treated cells, fixed and immunostained for EGFR (green) and endophilin (red) (images are representative of at least ten captures). Asterisks denote cells with strongly reduced endophilin levels. **h**, Plate reader quantification of BSC1 and RPE1 treated as in **g** (mean ± s.e.m., $n = 3$ independent experiments). **i**, Flow cytometry profiles of total EGFR levels in control (black) or TKD (red) cells. $n = 50{,}000$ cells for each conditions. **j**, Plate reader quantification of control or endophilin TKD BSC1 and RPE1 treated with 50 ng ml^{-1} EGF for the indicated time (mean ± s.e.m., $n = 3$ independent experiments). **k**, Confocal images of a BSC1 cell stimulated for 5 min with 250 ng ml^{-1} EGF, fixed and immunostained for EGFR (green) and endophilin (red) (images are representative of eight captures). Note that EPAs (arrowheads) are distinct from the large vacuole-like structures which are called macropinosomes, seen best in the middle confocal plane. Scale bars: 40 μm (**g**), 10 μm (**k**) and 5 μm (**a**–**c**).

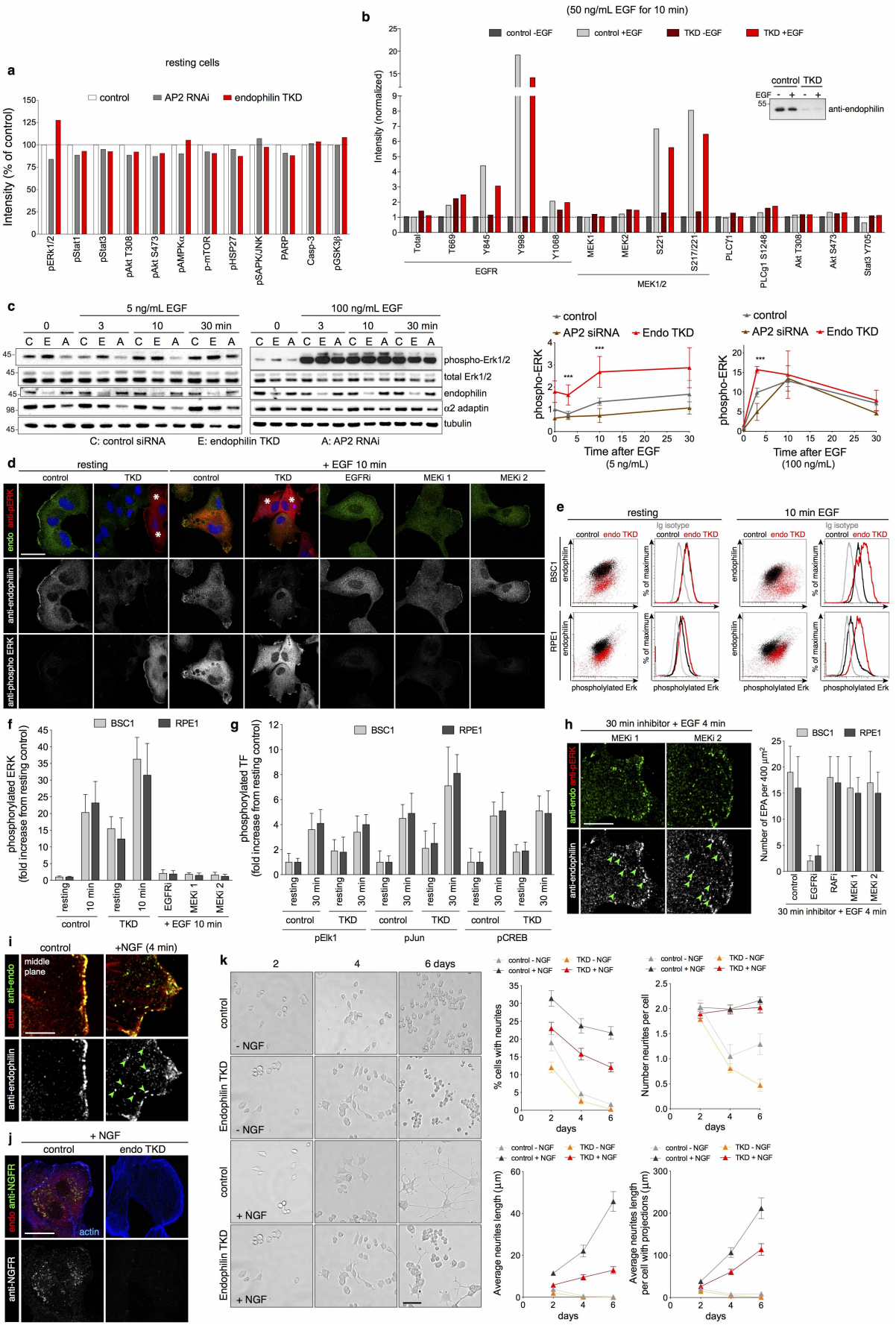

Extended Data Figure 7 | MAPK signalling and neurite outgrowth in endophilin TKD cells. Related to Fig. 2. **a**, Signals from PathScan antibody arrays reporting various intracellular signalling pathways. Intensities were normalized to the mean of the controls. Of all the signalling pathways tested endophilin TKD leads to a higher level of ERK phosphorylation (a component of the MAP kinase signalling cascade) in resting cells (mean, $n = 2$ independent experiments). **b**, Signals from PathScan antibody arrays reporting various steps within the EGFR signalling cascade. Intensities were normalized to the mean of the controls. The inset shows the level of endophilin knockdown in TKD cells. Endophilin TKD does not prevent phosphorylation of the EGFR at Y998 and thus does not account for defective endocytosis. Endophilin TKD does not prevent MEK phosphorylation on the RAF phosphorylation site (S217/S221), important for MEK activation (mean, $n = 2$ independent experiments). **c**, Immunoblots from control (C), endophilin TKD (E) or *AP2* RNAi (A) cells stimulated with 5 (left) or 100 ng ml^{-1} (right) EGF for the indicated times. Quantification of the signals from three independent experiments, normalized to the mean of the controls at $t = 0$ are shown below. As in **a** the resting pERK levels are increased in endophilin RNAi cells, probably because of an accumulation of receptors on the cell surface. At low concentrations of EGF (5 ng ml^{-1}) *AP2* RNAi largely prevents MAP kinase signalling while endophilin RNAi does not (but rather an enhanced level of signalling). At higher concentrations of EGF (100 ng ml^{-1}) there is much stronger signalling at an early time point in endophilin RNAi, pointing again to the importance of this pathway in reducing basal signalling (mean ± s.e.m., $n = 3$ independent experiments; $^{***}P < 0.001$, one-way ANOVA and Dunnett's test versus control $t = 0$). **d**, Confocal microscopy images of resting or stimulated (50 ng ml^{-1} EGF for 10 min) cells pre-treated with endophilin TKD (3 days) or the indicated inhibitors for 30 min before stimulation and immunostained for phosphorylated ERK1/2 (pERK, red), endophilin (green) and DNA (DRAQ5, blue) (images are representatives of at least ten captures). Asterisks denote cells with strongly reduced endophilin levels. **e**, Flow cytometry analysis of phosphorylated Erk1/2 levels in resting or stimulated (50 ng ml^{-1} EGF for 10 min) control (black) and endophilin TKD (red) cells. $n = 50{,}000$ cells for each conditions. **f**, Plate reader quantification of BSC1 or RPE1 cells treated as in **d**. Thus by immunoblotting and by immunostaining there is an increase in pERK in resting conditions in endophilin RNAi cells. Note the stronger increase in basal and stimulated pERK levels in endophilin TKD cells (mean ± s.e.m., $n = 3$ independent experiments). **g**, Plate reader quantification of control and endophilin TKD BSC1 or RPE1 cells resting or stimulated (50 ng ml^{-1} EGF for 30 min) and immunostained for phosphorylated Elk1, Jun or CREB (pElk1, pJun or pCREB) (mean ± s.e.m., $n = 3$ independent experiments). **h**, Left: confocal images (optical planes from the middle of cells) of BSC1 cells pre-treated with MEKi 1 or MEKi 2 for 30 min and stimulated with EGF (50 ng ml^{-1}, 4 min) and immunostained for endogenous endophilin-A (green) (images are representatives of six captures). Endophilin-positive puncta formation in response to growth factors is not dependent on MEK activation. Right: quantification of the number of endogenous EPAs per 400 μm^2 in BSC1 or RPE1 cells pre-treated for 30 min with the indicated inhibitors and stimulated with EGF (50 ng ml^{-1}, 4 min) (mean ± s.e.m., $n = 3$ independent experiments). **i**, NGF stimulates endophilin-positive puncta formation is RPE1 cells. Confocal images (optical planes from the middle of cells) of an RPE1 cell treated for 4 min with NGF (10 ng ml^{-1} for 4 min), fixed and immunostained for endogenous endophilin-A (green) (images are representatives of six captures). Cells were oriented with the leading edges (identified with phalloidin staining (actin, red)) pointing to the right. Arrowheads show internal vesicles positive for endogenous endophilin. **j**, Confocal images of cells treated with endophilin (endo TKD) or control siRNA and incubated with anti-NGFR antibodies (green) and 10 ng ml^{-1} NGF for 10 min at 37 °C, surface stripped on ice, fixed and immunostained for endophilin (red) and actin (blue) (images are representatives of eight captures). **k**, Neurite extension assays. PC12 cells pre-treated with control or endophilin TKD were stimulated or not with 100 ng ml^{-1} NGF for up to 6 days (images are representatives of at least 12 images). Quantifications show the percentage of cells with neurites (top left), average number of neurites per cell (top right), average neurite length (bottom left) and average neurite length per cell having neurites (bottom right) (mean ± s.e.m., $n = 3$ independent experiments). Scale bars: 40 μm (**d**), 20 μm (**k**) and 5 μm (**h**–**j**).

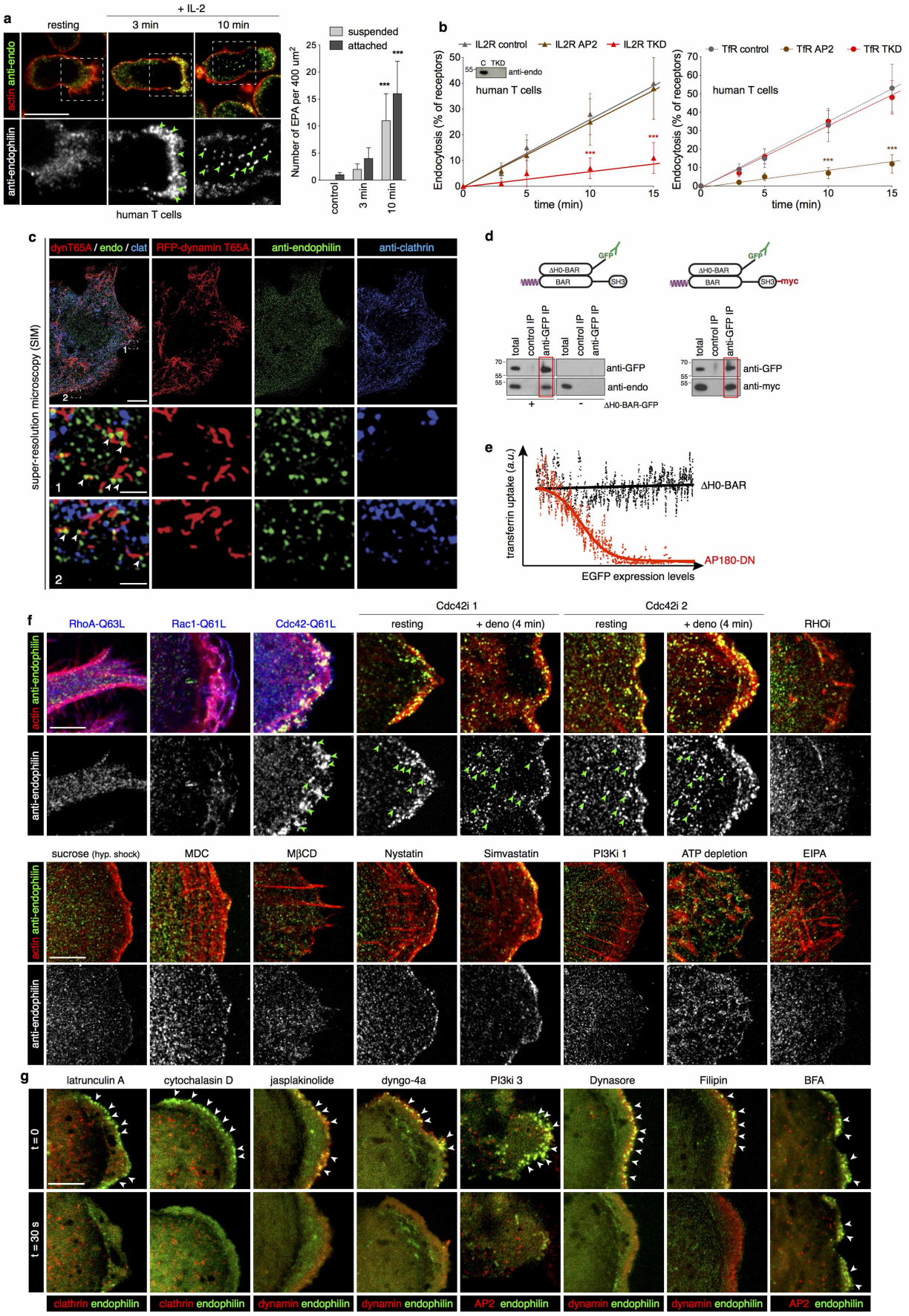

Extended Data Figure 8 | IL-2R uptake in endophilin TKD human T cells and chemical and genetic perturbations of FEME. Related to Figs 3 and 4. **a**, Confocal microscopy images (focal plane at the middle of cells) of human T cells immunostained for endogenous endophilin A (green) (images are representatives of at least ten images). Cells were either fixed directly ('resting') or 3 and 10 min after addition of IL-2 (500 pM). Scale bars, 5 μm (mean ± s.e.m., $n = 3$ independent experiments; $^{***}P < 0.001$, Student's t-test versus respective controls). **b**, Internalization rates of IL-2R and TfR in control, AP2 or endophilin TKD human T cells, measured by a plate reader (mean ± s.e.m., $n = 3$ independent experiments; $^{***}P < 0.001$, Student's t-test versus respective control time points). Inset: immunoblots of cell extracts used validated endophilin TKD. **c**, Super-resolution structured illumination microscopy (SIM) images of BSC1 cells overexpressing RFP-dynamin1-T65A mutant and immunostained for endophilin (green) and clathrin (blue) (images are representatives of at least five captures). Note that there was no leading edge in the presence of this dynamin mutant, and endophilin-positive assemblies were distributed across the plasma membrane. Dynamin1-T65A formed short tubules from the plasma membrane and at the tips of some of these tubules (arrowheads) in the boxed area (edges of cells) there were endophilin but not clathrin signals. **d**, Co-immunoprecipitation of ΔH0-BAR–EGFP with endogenous endophilin (red box, left) of with Myc-tagged overexpressed endophilin (red box, right). **e**, Flow cytometry profiles of internalized transferrin (Alexa546-labelled) in cells overexpressing increasing amounts of EGFP–AP180-DN (red) or ΔH0-BAR–EGFP (black). $n = 2{,}000$ cells for each condition. **f**, Confocal images of cells overexpressing the indicated mutants (blue) for 24 h or treated with the indicated inhibitors for 5 min before stimulation with 10 μM denopamine (4 min), fixed and immunostained for endogenous endophilin-A (green) and actin (phalloidin, red) (images are representative of at least six captures). Arrowheads point to EPAs. **g**, Live-cell confocal images before and after (+30 s) the addition of indicated inhibitors to cells expressing endophilin A2–RFP (green) and clathrin (EGFP–LCa, red) or dynamin (dynamin 2–EGFP, red) (images are representatives of at least three captures from independent experiments). Arrowheads point to endophilin spots. Scale bars: 10 μm (**a**, **c**), 5 μm (**f**, **g**) and 1 μm (**c**, insets).

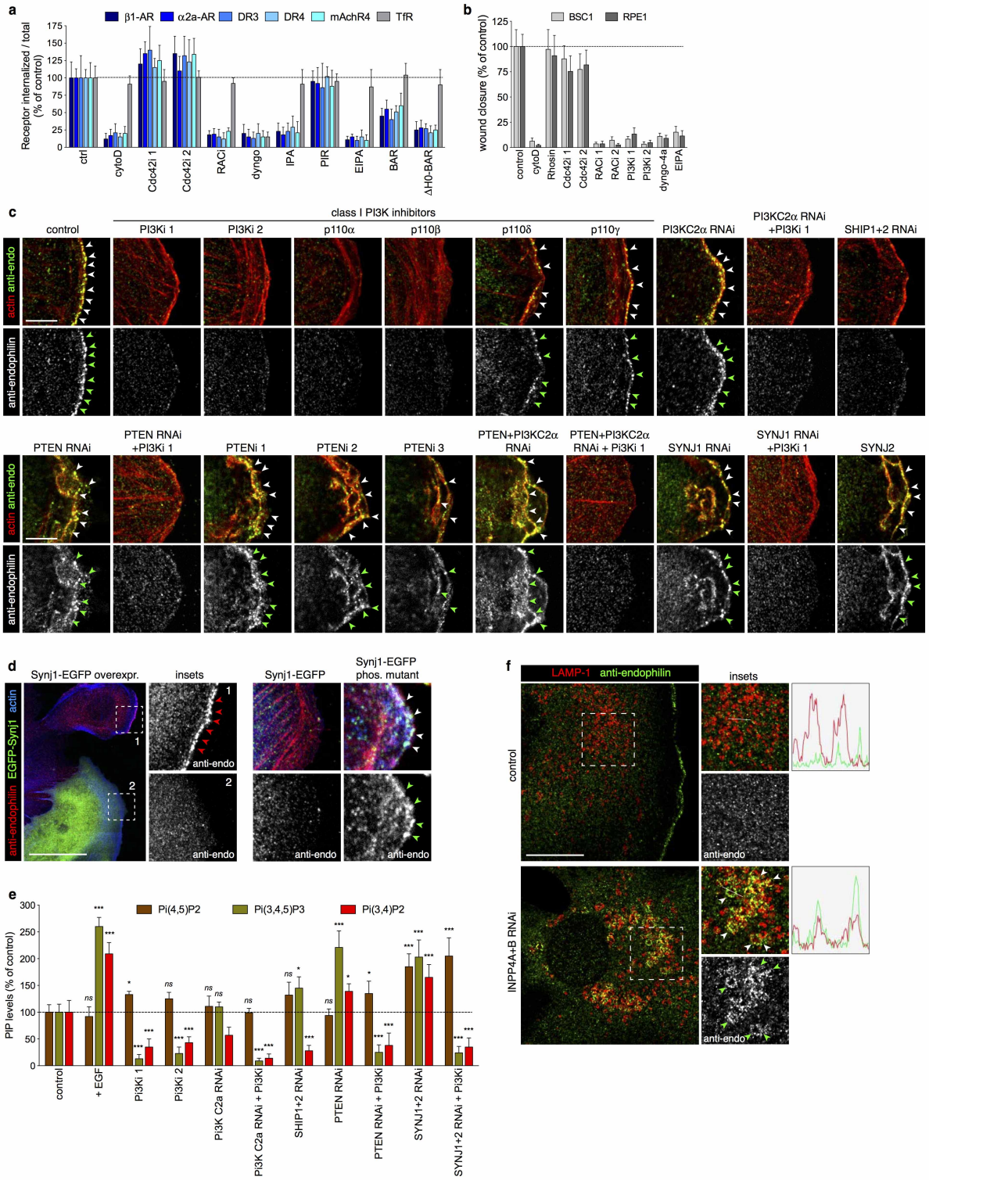

Extended Data Figure 9 | The recruitment of endophilin at leading edges of cells requires PtdIns(3,4)P_2. Related to Fig. 5. **a**, Receptor uptake assay (HA–receptor–EGFP internalized, corrected for total levels) in cells treated with the depicted inhibitors (mean ± s.e.m., $n = 3$ independent experiments). **b**, Wound-closure assay. BSC1 and RPE1 cell monolayers were wounded and cell migration into the wound sites were assessed after 16 h. The inhibitors were added just after wounding (mean ± s.e.m., $n = 3$ independent experiments). **c**, Confocal images of cells treated with the indicated inhibitors or RNAi, fixed and immunostained for endogenous endophilin-A (green) and actin (phalloidin, red) (images are representative of at least six captures from three independent experiments). Arrowheads point to endophilin foci at the leading edges of cells. **d**, Confocal images of cells overexpressing the indicated constructs fixed and immunostained for endogenous endophilin-A (red) and actin (phalloidin, blue) (images are representative of at least six captures from three independent experiments). **e**, Quantifications of PtdIns(4,5)P_2 (mocha), PtdIns(3,4)P_2 (red) or PtdIns(3,4,5)P_3 (asparagus) levels from cells treated with the indicated siRNA and PI(3)K inhibitor, immunostained for the lipids and measured using a plate reader (mean ± s.e.m., $n = 3$ independent experiments; NS, non-significant; $^*P < 0.05$; $^{***}P < 0.001$, one-way ANOVA and Dunnett's test versus respective control levels). **f**, Confocal images of cells treated with *INP4A* and *INP4B* or control siRNA, fixed and immunostained for endogenous endophilin-A (green) and LAMP-1 (red) (images are representative of at least six captures from three independent experiments). Intensity profiles were acquired along the indicated lines. Scale bars: 20 μm (**d**), 10 μm (**f**) and 5 μm (**c**).

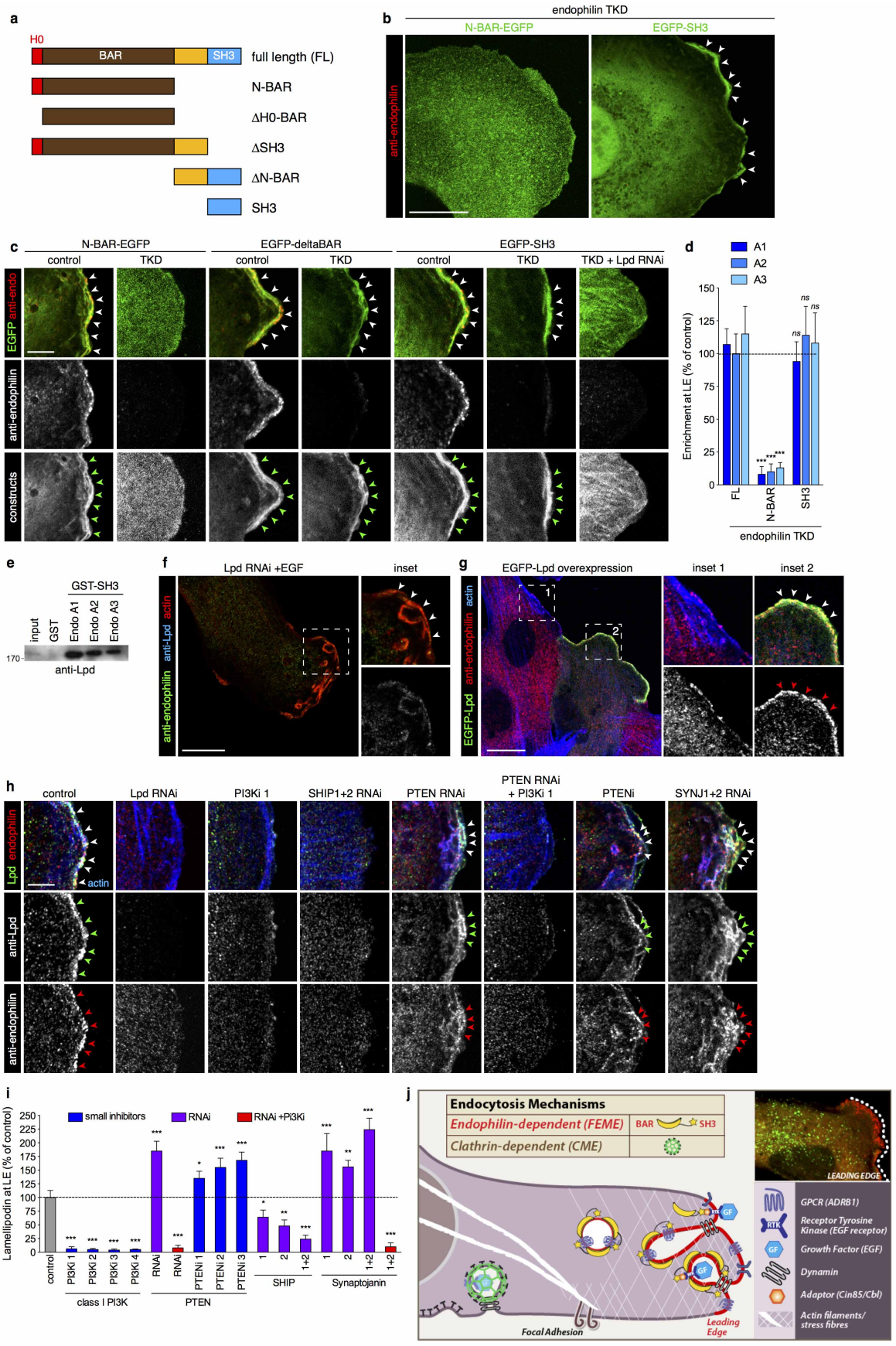

Extended Data Figure 10 | Lamellipodin recruits endophilin at the leading edge. Related to Fig. 5. **a**, Scheme depicting the endophilin constructs used. **b**, **c**, Confocal images of cells depleted for endogenous endophilin (TKD) or not (control siRNA) and expressing the indicated constructs, fixed and immunostained for endogenous endophilin to ascertain the depletion in the cells imaged (images are representatives of at least six captures from three independent experiments). **d**, Quantification of construct levels at the leading edges of cells depleted of endogenous endophilin (TKD) and expressing the indicated endophilin constructs (mean ± s.e.m., $n = 3$ independent experiments; NS, non-significant; $^{***}P < 0.001$ one-way ANOVA and Dunnett's test versus respective full-length levels). **e**, Pull-down experiments using GST–SH3 domains of endophilin-A1, 2 or 3 (or GST as a control) with EGFP–lamellipodin. 10% of cell extract was used as 'input'. **f**, Confocal image of cell depleted for lamellipodin (lpd) and treated with 200 ng ml^{-1} EGF for 5 min to stimulate PI(3)K and induce ruffles, fixed and immunostained for endophilin (green), actin (red) and lamellipodin (blue, to ascertain the depletion) (images are representatives of at least six captures from three independent experiments). **g**, Confocal image of a cell overexpressing EGFP–lamellipodin next to a non-transfected cell, fixed and immunostained for endophilin (red) and actin (blue) (images representatives of at least six captures from three independent experiments). **h**, Confocal images of cells treated with the indicated RNAi and inhibitors, fixed and immunostained for lamellipodin (green), endophilin (red) and actin (blue) (images representatives of at least six captures from three independent experiments). **i**, Quantification of levels of endogenous lamellipodin at the leading edges of cells treated with the indicated small inhibitors (blue), RNAi (purple), RNAi plus class I PI(3)K inhibitor ('PI3Ki', GDC-0941, 50 nM for 5 min; red) (mean ± s.e.m., $n = 3$ independent experiments; NS, non-significant; $^{*}P < 0.05$, $^{**}P < 0.01$, $^{***}P < 0.001$ one-way ANOVA and Dunnett's test versus control). **j**, Model: endophilin-dependent (FEME) endocytosis from the leading edge. Endophilin-coated vesicles/tubules associate with receptors (after ligand binding) or receptor-adaptors (like CIN85/Cbl) via their SH3 domains, and promote membrane curvature with their N-terminal N-BAR domains. Vesicle scission is promoted by dynamin, which is also recruited by endophilin. Scale bars: 20 μm (**b**, **g**), 10 μm (**f**) and 5 μm (**c**, **h**).

Video

1. Video 1: Spinning-disk confocal microscopy of a BSC1 cell stably expressing σ2-EGFP (AP2, green) and transiently expressing low levels of endophilin A2-RFP (red) and imaged at 0.5 Hz. (6.29 MB, Download)
   The cell was imaged at 37 °C in normal imaging medium (5 % serum). Note the numerous endophilin puncta devoid of AP2 at the leading edge of the cell. The video is playing at 10 frames/sec.

2. Video 2: Spinning-disk confocal microscopy of a confluent BSC1 cell transiently expressing low levels of EGFP-LCa (clathrin, green) and endophilin A2-RFP (red) and imaged at 2 Hz. (6.02 MB, Download)
   The cell was imaged at 37 °C in normal imaging medium (5 % serum). Note the numerous endophilin puncta devoid of clathrin. The video is playing at 10 frames/sec.

3. Video 3: Spinning-disk confocal microscopy (focal plane ~1 µm above the bottom surface) of a BSC1 cell transiently expressing low levels of endophilin A2-RFP (red) and imaged at 0.5 Hz. (28.49 MB, Download)
   The cell was imaged at 37 °C in normal imaging medium (5 % serum). Additional 10 µM isoproterenol was added at the time frame 5. Note the numerous endophilin-coated tubules and vesicles budding from the periphery of the cell and accumulating toward the perinuclear area. The video is playing at 10 frames/sec.

4. Video 4: Spinning-disk confocal microscopy (focal plane ~1 µm above the bottom surface) of a BSC1 cell transiently expressing low levels of endophilin A2-RFP (red) and imaged at 0.5 Hz. (16.34 MB, Download)
   The cell was imaged at 37 °C in serum-free imaging medium (changed right before imaging). Additional 2 ng/mL was added at the time frame 0. Note the numerous endophilin-coated tubules and vesicles budding from the periphery of the cell and moving toward the perinuclear area. The video is playing at 10 frames/sec.

5. Video 5: Spinning-disk confocal microscopy (focal plane ~1 µm above the bottom surface) of a BSC1 cell transiently expressing endophilin A2-RFP (red) and Cdc42-T17N dominant negative mutant and imaged at 0.5 Hz. (13.56 MB, Download)
   The cell was imaged at 37 °C in normal imaging medium (5 % serum). Note the recruitment of endophilin all around the edge of the cell and the numerous endophilin-coated tubules and vesicles budding from the periphery of the cell even though the cell was not stimulated with additional growth factor or β1-AR agonist. The video is playing at 10 frames/sec.